The Finite-Amplitude Nature of Tropical Cyclogenesis

KERRY A. EMANUEL

Center for Meteorology and Physical Oceanography, Massachusetts Institute of Technology, Cambridge, Massachusetts

(Manuscript received 2 February 1989, in final form 30 May 1989)

ABSTRACT

We have constructed a simple, balanced, axisymmetric model as a means of understanding the existence of the threshold amplitude for tropical cyclogenesis discovered by Rotunno and Emanuel. The model is similar to Ooyama's but is phrased in Schubert and Hack's potential radius coordinates.

The essential difference between this and other balanced models lies in the representation of convective clouds. In the present model the cumulus updraft mass flux depends simply and directly on the buoyancy (on angular momentum surfaces) of lifted subcloud-layer air and is not explicitly constrained by moisture convergence. The downdraft mass flux is equal to the updraft flux multiplied by $(1-\epsilon)$, where ϵ is the precipitation efficiency. The complete spectrum of convective clouds in nature is here represented by two extremes: deep clouds with a precipitation efficiency of one, and shallow, nonprecipitating clouds. The former stabilize the atmosphere both by heating the free atmosphere and drying out the subcloud layer, whereas the shallow clouds stabilize only through drying of the subcloud layer. The two cloud types may coexist. In the crude vertical structure of the model, shallow clouds have the same thermodynamic effect as precipitation-induced downdrafts. Model runs without shallow clouds but with precipitation-induced downdrafts produce the same qualitative features as the runs with shallow clouds.

The existence of low-precipitation-efficiency clouds is crucial to the model hurricane development. When a weak vortex is placed in contact with the sea surface, the enhanced surface fluxes together with adiabatic cooling induced by Ekman pumping destabilize the atmosphere. The initial convective clouds that form have relatively low precipitation efficiency and thus only partially compensate for the adiabatic cooling associated with the Ekman pumping. They do, however, import low θ_e air into the subcloud layer. The vortex core therefore cools and the vortex decays. Only when the anomalous surface fluxes are strong enough, and/or the middle troposphere humid enough does the subcloud layer θ_e increase, and with it the temperature of the core and the amplitude of the cyclone.

The low-precipitation-efficiency clouds play a dual role, however. Once amplification begins, these clouds continue to dominate the convection outside the eyewall, keeping the boundary layer θ_e relatively low. Without low-precipitation-efficiency clouds, large heating occurs in the outer region and the vortex expands and weakens.

1. Introduction

Tropical weather forecasters have long known that tropical cyclones arise out of preexisting disturbances such as easterly waves or cyclonic disturbances on fronts that penetrate the tropics (Anthes 1982; Riehl 1954). Only when certain necessary conditions are fulfilled will tropical cyclones develop (Gray 1968), but even when these conditions are met only a small percentage of potential initiating disturbances result in tropical storms (Bergeron 1954). Sufficient conditions for tropical cyclogenesis remain enigmatic.

In spite of forecasting experience, early genesis theories assumed that the mean state of the tropical atmosphere is linearly unstable to tropical cyclone-like disturbances. The problem for the early theorists was principally one of explaining the scale of the incipient cyclones, since conditional instability always gives rise to disturbances of very small horizontal scale (see Yanai 1964). The work of Ooyama (1964) and Charney and Eliassen (1964) attempted to overcome this problem by relating heating to vertical velocity at the top of the boundary layer. Depending on the choice of the vertical distribution of heating, growing disturbances with finite scale can be obtained. Numerical simulations made by Anthes (1972a) showed that axisymmetric models could produce realistic tropical cyclones starting from very small perturbations in a conditionally unstable atmosphere.

Common to all the early theories, including Conditional Instability of the Second Kind (CISK), is the assumption that the tropical atmosphere is conditionally unstable and that tropical cyclones result from a *linear* instability in which infinitesimal disturbances grow from the mean state of the tropical atmosphere. The existence of an energy reservoir associated with conditional instability has been challenged by Betts (1982) and Xu and Emanuel (1989). They showed that soundings from the deep tropics are nearly neutral

Corresponding author address: Dr. Kerry A. Emanuel, Center for Meteorology and Physical Oceanography, Massachusetts Institute of Technology, Cambridge, MA 02139.

to reversible ascent in the lower and middle troposphere. Xu and Emanuel (1989) demonstrate that the density of a reversibly displaced parcel from the subcloud layer is the *minimum* that can be obtained in a nonprecipitating cloud and that the reversible moist adiabat is thus the appropriate measure of marginal stability in the tropical atmosphere. As marginal stability characterizes all very high Reynolds number convection, it is not surprising that the convective tropical atmosphere exhibits marginally stable soundings. The maintenance of a moist-neutral state is also the basis of the Arakawa–Schubert (1974) convective representation. Without convective available potential energy, the energy for the CISK process is absent.

In contrast to genesis theories, explanations of the maintenance of mature hurricanes have recognized for almost 40 years the importance of the oceanic heat source (e.g., see Kleinschmidt 1951; Riehl 1954). The paramount role of heat transfer from the ocean was conclusively established by Ooyama (1969), and Emanuel (1986) demonstrated that the intensity of mature tropical cyclones could be explained without reference to ambient conditional instability. The thermodynamic disequilibrium between ocean and atmosphere is now universally recognized as the energy source of mature tropical cyclones.

The lack of an observational basis for the idea that tropical cyclones develop from a linear instability, together with the absence of a significant reservoir of convective energy in the tropics, led Emanuel (1986) to propose that tropical cyclones result from a finite-amplitude instability involving the feedback between the cyclone and wind-induced evaporation. This idea was tested by Rotunno and Emanuel (1987; hereinafter referred to as RE), who performed numerical integrations with a nonhydrostatic primitive-equation model that explicitly resolves convective clouds. The model atmosphere was preconditioned by allowing convective clouds to grow and decay until a convectively neutral state was achieved. A finite-amplitude vortex was then placed in the neutral atmosphere.

The principal finding of RE was that weak initial vortices decay while sufficiently strong ones amplify into mature tropical cyclones, provided their initial horizontal scale is not too large. This finding is well in accord with the observation that even when the necessary conditions are satisfied, real tropical cyclones do not arise spontaneously but invariably develop out of preexisting disturbances of presumably independent dynamical origin.

It is the purpose of the present work to explore the reasons for the finite-amplitude behavior found in the simulations of RE. Rather than attempt to infer these reasons from the complex fields of a complete model, we have elected to construct a far simpler model that retains only the essential physics. By omitting certain physical processes, one can hope to discover just what is and what is not essential. In section 2 we describe the model in detail and discuss the model's sensitivity to numerical parameters such as resolution and viscosity. The principal results of this work are presented in section 3, in which the finite-amplitude behavior of the model vortex is explored. The sensitivity of the model to other parameters such as initial vortex geometry and middle tropospheric moisture is discussed in section 4. Section 5 contains concluding remarks.

2. Description of the model[1]

The basic design of the simplified model is similar to that of Ooyama (1969) except that it is phrased in angular momentum coordinates and contains a representation of cumulus convection that is based on local conditional (slantwise) instability alone and does not explicitly depend on moisture convergence. The initial state of the model is one of (slantwise) conditional neutrality, as in RE. The model assumes the atmosphere on the cyclone scale to be in gradient wind and hydrostatic balance.

The heart of the model is described in this chapter. For the reader uninterested in the details of the model, the dimensionless equations are summarized in section 2i, while the scaling and model parameters are listed in Tables 1 and 2. Section 2a and Fig. 1 describe the model's structure. The schema of this section is as follows:

a. Coordinate system and model structure
b. Balance condition
c. Conservation of mass
d. Conservation of angular momentum
e. Saturation entropy
f. Conservation of entropy (θ_e)
g. Representation of cumulus convection
h. Scaling appropriate for air–sea interaction systems
i. Summary of dimensionless model equations and parameters
j. Boundary and initial conditions and numerical scheme.

In sections 2a–g the final results of derivations are enclosed in boxes.

a. Coordinate system and model structure

The model is time dependent and axisymmetric, with the two spatial coordinates being pressure and "potential radius," R. The latter variable was defined

[1] The model is written in standard FORTRAN 77 and is highly documented. It is designed to be completely transportable and "user friendly" and may be run on personal computers. The control simulation described herein, when run to 12 time units (approximately 190 simulated hours), uses 1 minute, 13 seconds of CPU time on a DEC VAX 8550. The model is available from the author for the cost of reproduction and mailing.

by Schubert and Hack (1983) as the radius at which a parcel would attain zero tangential velocity if displaced radially while conserving angular momentum. It is proportional to the square root of the absolute angular momentum per unit mass:

$$\frac{f}{2}R^2 \equiv rV + \frac{f}{2}r^2, \tag{1}$$

where f is the Coriolis parameter (assumed constant), r the radius from the storm center, and V the azimuthal velocity.

There are three reasons for using R as the model's radial coordinate. Since R is conserved in the absence of friction, the only radial advections in R coordinates will be due to frictional dissipation. Second, R surfaces will become densely packed in regions of high vorticity such as the eyewall, although regions of anticyclonic relative vorticity will be relatively poorly represented. The main reason for using R coordinates, however, is that we will suppose that moist convection generally acts to reduce the atmosphere to a state of neutrality along angular momentum (R) surfaces, rather than in the vertical. This appeared to be true in the model simulations of RE with explicit convection, and has been observed to be the case in middle-latitude cyclones (Emanuel 1988a). Kleinschmidt (1951) assumed this to be the case in tropical cyclones. By using R coordinates, a relaxation to moist adiabatic lapse rates in the model's vertical coordinate is, in effect, a relaxation along angular momentum surfaces. This process is described in section 2g.

The vertical structure of the model is illustrated in Fig. 1. A mass streamfunction, ψ, is calculated at the middle level of the model from a Sawyer–Eliassen equation (section 2j). The streamfunction at the top of the boundary layer (ψ_0) is diagnosed from a nonlinear Ekman-layer formulation described in section 2d. The model's temperature variable is saturation moist entropy, s^*, which is the moist entropy the atmosphere would have if it were saturated while holding temperature and pressure constant. It is defined approximately (neglecting effects of water substance on heat capacities, etc.) by

$$s^* = c_p \ln T + \frac{L_v r^*}{T} - R \ln \frac{p}{p_0},$$

where T and p are temperature and pressure, p_0 a reference pressure, r^* the saturation mixing ratio, L_v the heat of vaporization, and c_p and R are the heat capacity at constant pressure and gas constant. Neglecting effects of variable water content, density may be regarded as a function of pressure and s^* alone. The saturation moist entropy is related to saturation equivalent potential temperature, θ_e^*, by

$$s^* = c_p \ln \theta_e^*.$$

The state of slantwise conditional neutrality is characterized by constant s^* (moist adiabatic temperature lapse rate) along angular momentum surfaces, with s^* equal to the actual moist entropy, s, in the boundary layer (again neglecting the effect of variable water content on density). Thus we take s^* to be approximately uniform along R surfaces, as discussed above. For convenience, we ascribe its value to the model's middle level. An additional temperature variable, s_m^*, is predicted at the middle of the lower layer. Its value is used only to predict the shallow clouds and does not directly affect the model dynamics.

The moist entropy itself is defined in the model's subcloud layer (s_b) and in the middle of the lower tropospheric layer (s_m). Entropy is related to equivalent potential temperature by

$$s = c_p \ln \theta_e.$$

The subcloud-layer entropy is controlled by surface fluxes, radial advection across R surfaces due to the sink of angular momentum in the boundary layer, fluxes by the mean flow through the top of the boundary layer, and exchange of entropy by shallow cumulus clouds. The prediction of lower-tropospheric entropy (s_m) turns out to be crucial to the budget of subcloud-layer entropy, which in turn influences the cloud mass fluxes, as described in section 2g.

The two variables related to azimuthal (tangential) velocity are r_b and r_t, the physical radii of R surfaces where they intersect the top of the subcloud layer and the tropopause, respectively. Knowledge of R and r is sufficient to determine the local azimuthal velocity.

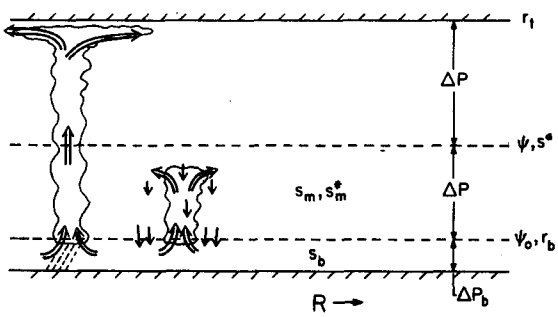

FIG. 1. Vertical structure of numerical model. Streamfunction is defined at the middle level and top of the subcloud layer and physical radius is calculated at the top and at the subcloud layer. The temperature variable, s^*, represents a vertically averaged value but is ascribed to the middle level. Entropy, s, is calculated in the subcloud layer and within the lower-tropospheric layer. The subsidiary temperature variable, s_m^*, is used to predict the shallow cumulus activity. Deep clouds lift mass from the subcloud layer to the top layer while shallow clouds exchange entropy between the lower troposphere and the subcloud layer without producing a net mass flux.

b. *Balance condition*

The fundamental balance condition of the model is the thermal wind relation obtained by assuming slant-

wise neutrality and hydrostatic and gradient balance as derived by Emanuel (1986). It may be written

$$\boxed{\frac{1}{r_b^2} = \frac{1}{r_t^2} - \frac{2}{f^2R^3}(T_s - T_t)\frac{ds^*}{dR},} \tag{2}$$

where T_s and T_t are the absolute temperatures of the sea surface and tropopause, respectively. Each of these temperatures is held constant. The derivation of (2) assumes that s^* is constant along R surfaces; this is the condition of slantwise neutrality (Emanuel 1988a). To the extent that s^* is not constant, it may be taken to be the vertically averaged value in the model. The relation (2) shows that when the radial gradient of s^* is negative, the R surfaces slope outward with height ($r_t > r_b$), implying anticyclonic shear.

c. Conservation of mass

The conservation equations in this model are formulated in a way that explicitly separates variables outside of convective clouds from those inside the clouds, as originally suggested by Raymond (1983). The fields outside of clouds are calculated explicitly, while those on the inside are parameterized. The conservation equations of the model therefore pertain to flow outside of clouds and the clouds themselves appear as sources and sinks of mass and entropy (but not momentum since we implicitly account for this by convecting along angular momentum surfaces).

In physical cylindrical coordinates, the hydrostatic form of the mass continuity equation has the form

$$\frac{1}{r}\frac{\partial}{\partial r}(ru) + \frac{\partial}{\partial p}[(1-\sigma)\omega_a] = -\frac{\partial}{\partial p}(\sigma\omega_c), \tag{3}$$

where u is the radial velocity averaged over both cloud and noncloud areas, ω_a and ω_c are the Lagrangian time derivatives of pressure (the vertical velocities) in the environment of clouds and within clouds, respectively, and σ is the fractional areal coverage of convective clouds. *The right-hand side of (3) represents mass sources and sinks due to convective clouds and will be parameterized as described in section 2g.*

It proves convenient to replace the variables u and $(1-\sigma)\omega_a$ by new variables ψ and G, defined as follows:

$$\boxed{ru \equiv \frac{\partial\psi}{\partial p} - \frac{\partial G}{\partial p},} \tag{4}$$

$$\boxed{(1-\sigma)r\omega_a \equiv -\frac{\partial\psi}{\partial r}.} \tag{5}$$

The variable ψ will be a mass streamfunction in the r–p plane in the absence of convection. Substitution of (4) and (5) into (3) shows that G is related to the cumulus mass flux by

$$\boxed{G \equiv \int_0^r \sigma\omega_c r'dr'.} \tag{6}$$

Thus G is the radially integrated cumulus mass flux. Although (4) and (5) are expressed in physical coordinates, the variables ψ and G will naturally appear in the transformed system, as will be shown presently.

d. Conservation of angular momentum

A relation expressing angular momentum conservation is easily derived from the definition of radial velocity:

$$\frac{dr}{dt} \equiv u = \frac{1}{r}\frac{\partial\psi}{\partial p} - \frac{1}{r}\frac{\partial G}{\partial p}, \tag{7}$$

where the latter equality comes from (4). Using the chain rule, the above can be transformed into potential-radius coordinates, resulting in

$$\frac{\partial r^2}{\partial\tau} + \frac{dR}{dt}\frac{\partial r^2}{\partial R} = 2\left(\frac{\partial\psi}{\partial P} - \frac{\partial G}{\partial P}\right), \tag{8}$$

where the new coordinates are time (τ), pressure (P), and potential radius (R). Partial derivatives with respect to τ and P hold R rather than r fixed. Terms involving the vertical advection (dP/dt) cancel between the left- and right-hand sides of (8).

We next specialize (8) to the top, bottom, and boundary layers indicated in Fig. 1. In the top layer, we assume no friction ($dR/dt = 0$) as there is no solid boundary there (and thus no Ekman pumping) and since no internal diffusion seems to be necessary for numerical stability. In this layer we approximate the derivative in (8) by finite differences:

$$\boxed{\frac{\partial r_t^2}{\partial\tau} = \frac{2\psi - 2G}{\Delta P},} \tag{9}$$

where r_t is the physical radius at the top of the model, ΔP the pressure difference across each of the main model layers, and G the integrated cumulus mass flux at the middle level. The variable ψ is now the streamfunction at the middle level and ψ and G are assumed to vanish at the model top.

In the bottom layer, we include radial diffusion of momentum (see section 3b). From the definition of potential radius (1), we have

$$fR\frac{dR}{dt} = \frac{dM}{dt} = rD_v, \tag{10}$$

where M is the absolute angular momentum and D_v is the frictional drag. We use an eddy viscosity formulation for D_v, as in RE. This gives

$$D_v = \frac{1}{r_b^2}\frac{\partial}{\partial r_b}\left(r_b^3\nu\frac{\partial}{\partial r_b}\left(\frac{v}{r_b}\right)\right)$$

$$= \frac{f}{2r_b^2}\frac{\partial}{\partial r_b}\left(r_b^3\nu\frac{\partial}{\partial r_b}\left(\frac{R^2}{r_b^2}\right)\right), \tag{11}$$

with the eddy viscosity related to the local deformation by

$$\nu = l^2\left|\frac{\partial V}{\partial r_b} - \frac{V}{r_b}\right| = \frac{f}{2} l^2 r_b \left|\frac{\partial}{\partial r_b}\left(\frac{R^2}{r_b^2}\right)\right|, \quad (12)$$

where l is a length scale. Here r_b is the physical radius at the top of the subcloud layer. With this formulation, and representing vertical derivatives by finite differences, (8) becomes in the lower layer

$$\boxed{\frac{\partial r_b^2}{\partial \tau} = -2\frac{\psi - \psi_0}{\Delta P} - \frac{1}{R}\frac{\partial}{\partial R}\left(r_b^3 \nu \frac{\partial}{\partial r_b}\left(\frac{R^2}{r_b^2}\right)\right),} \quad (13)$$

with ν given by (12) and where ψ_0 is the streamfunction at the top of the boundary layer, to be discussed presently. We have also assumed that the divergence of the cumulus mass flux vanishes in the lower layer (as discussed in section 2g), with all the mass inflow coming from the subcloud layer.

In the boundary layer itself, we shall assume that the frictional term in (8) is quite large compared to the local time derivative. We therefore approximate (8) by a balance between inward advection and destruction of angular momentum. The drag term, D_v, in (10) is approximated by the vertical divergence of the vertical flux of angular momentum:

$$D_v = g\frac{\partial F_v}{\partial P}, \quad (14)$$

where g is the acceleration of gravity and we assume that $\partial/\partial P \approx \partial/\partial p$; i.e., that there is little baroclinity in the boundary layer. Here F_v is the azimuthal stress. Using (14) and ignoring the time derivative in (8), the latter becomes

$$\frac{\partial \psi}{\partial P} = \frac{\partial G}{\partial P} + \frac{g}{2}\frac{r}{fR}\frac{\partial r^2}{\partial R}\frac{\partial F_v}{\partial P}. \quad (15)$$

We again make the reasonable assumption that R surfaces are nearly vertical in the boundary layer, so that $r \neq r(P)$. Then (15) may be integrated through the depth of the boundary layer to give

$$\boxed{\psi_0 = G - \frac{g}{2}\frac{r_b}{fR}\frac{\partial r_b^2}{\partial R}F_{vs},} \quad (16)$$

where F_{vs} is the azimuthal surface stress, and we have assumed that the turbulent stress vanishes at the top of the boundary layer.

The boundary-layer formulation (16) states that the flow through the top of the boundary layer is the sum of that needed to balance the cumulus mass flux out of the boundary layer and the radial gradient of the frictional stress as in classical Ekman layers.

As in RE, the surface stress is calculated using the aerodynamic drag law,

$$\boxed{F_{vs} = -\rho_0 C_D |V_b| V_b,} \quad (17)$$

where ρ_0 is a mean surface density and C_D is a drag coefficient, which (as in RE) is given by Deacon's formula:

$$\boxed{C_D = C_{D0} + C_{D1}|V_b|,} \quad (18)$$

where C_{D0} and C_{D1} are constants. The wind speed V_b in (17) and (18) is approximated by the azimuthal wind at the top of the boundary layer. The dependence of C_D on $|V_b|$ reflects the dependence of surface roughness on wind speed over the ocean. We include this wind dependence based on its importance in RE and its inclusion in similar balanced models, such as that of Ooyama (1969).

e. *Saturation moist entropy*

The saturation moist entropy, s^*, is the model's central temperature variable and is directly linked to the circulation through the thermal wind relation, (2). We do not separate this variable into in-cloud and out-of-cloud parts, but instead use the approximation that the temperature in clouds is approximately the same as that of their environment.

The equation for the areally averaged dry entropy, s_d, is

$$\frac{\partial s_d}{\partial \tau} + (1-\sigma)\omega_a\frac{\partial s_d}{\partial P} = D_{s_d} + \dot{H} - \sigma\omega_c\left(\frac{\partial s_d}{\partial P}\right)_c, \quad (19)$$

where $\dot{H}$ represents convective heating and radiational cooling and D_{s_d} is a radial diffusion term that was found to be necessary to prevent discontinuities from forming. The term $(\partial s_d/\partial P)_c$ is the lapse rate of dry entropy inside of clouds.

Following Arakawa and Schubert (1974), we assume that most of the actual local temperature change is due to subsidence outside of clouds, and that heating in clouds is very nearly balanced by adiabatic cooling; i.e.,

$$\sigma\omega_c\left(\frac{\partial s_d}{\partial P}\right)_c \approx \dot{H} - \dot{H}_{\text{rad}},$$

where $\dot{H}_{\text{rad}}$ is the radiative heating.

As the temperature is only predicted at one level in the model, we must take the static-stability term to be a constant in (19). Since the temperature lapse rate has already been assumed to be moist adiabatic on R surfaces, the static stability itself will be in practice a weak function of temperature.

Finally, we relate changes in saturation moist entropy (s^*) at constant pressure to changes in s_d using an elementary relation of moist thermodynamics derived in Emanuel (1986):

$$(\delta s^*)_p = \frac{\Gamma_d}{\Gamma_m}(\delta s_d)_p,$$

where Γ_d and Γ_m are the dry and moist adiabatic lapse rates, respectively. Then (19) may be written

$$\frac{\partial s^*}{\partial \tau} + \frac{\Gamma_d}{\Gamma_m}(1-\sigma)\omega_a \frac{\partial s_d}{\partial P} = D_{s^*} + \frac{\Gamma_d}{\Gamma_m}\dot{H}_{\text{rad}}. \quad (20)$$

As in RE, we use an eddy diffusion formulation for D_{s^*} and Newtonian cooling for $\dot{H}_{\text{rad}}$:

$$D_{s^*} = \frac{1}{r_b}\frac{\partial}{\partial r_b}\left(r_b \nu \frac{\partial s^*}{\partial r_b}\right), \quad (21)$$

and

$$\frac{\Gamma_d}{\Gamma_m}\dot{H}_{\text{rad}} = -\text{rad}(s^* - s_i^*), \quad (22)$$

where rad is a Newtonian relaxation rate and s_i^* is the saturation moist entropy of the basic state. The variable r_b is used throughout (21) rather than some vertically interpolated value of r; this was found to be necessary to prevent discontinuities from forming at the top of the boundary layer. A cap is placed on $\dot{H}_{\text{rad}}$ in (22) so that the cooling rate does not exceed about 2°C per day, and as a crude means of incorporating the infrared absorption by clouds, we turn off the radiative cooling where the Ekman pumping is upward.

We also predict saturation moist entropy (s^*) in the middle of the lower layer for the sole purpose of calculating the shallow cumulus mass flux (see section 2g). We do not include a diffusion term here, and interpolate the vertical velocity between the middle level and the top of the boundary layer:

$$\frac{\partial s_m^*}{\partial \tau} + \frac{1}{2}\frac{\Gamma_d}{\Gamma_m}\frac{\partial s_d}{\partial P}(1-\sigma)(\omega_a + \omega_{a0}) = -\text{rad}(s_m^* - s_{mi}^*). \quad (23)$$

Because the Ekman pumping

$$\omega_{a0} = -(1-\sigma)\frac{1}{r_b}\frac{\partial \psi_0}{\partial r_b}$$

is diagnosed rather than predicted, and because s_m^* has no direct dynamical feedback, it was found that s_m^* calculated from (23) becomes absurdly large in regions of Ekman suction. Therefore we impose the condition that s_m^* must be no larger than s^*:

$$s_m^* \leq s^*. \quad (24)$$

We also note that ω_a in (20) and (23) is evaluated at the model's middle level. From (5),

$$(1-\sigma)\omega_a = -\frac{1}{r_i}\frac{\partial \psi}{\partial r_i}, \quad (25)$$

where r_i is the radius of R surfaces at the middle level. The value of r_i may be obtained from a thermal wind equation similar to (2):

$$\frac{1}{r_i^2} = \frac{1}{r_b^2} + \frac{2}{f^2 R^3}(T_s - T_m)\frac{ds^*}{dR}, \quad (26)$$

where T_m is a characteristic absolute temperature at the middle level.

f. Conservation of moist entropy (θ_e)

The conserved thermodynamic variable in moist atmospheres is moist entropy, which is the sum of the entropies of dry air, water vapor, and condensed water [an exact definition valid in both saturated and unsaturated air may be found in Emanuel (1988b)]. Total entropy can be gained from the sea surface (the principal energetic process in tropical cyclones) and lost by radiation to space. Frictional dissipation can also raise the entropy, but this is usually a small effect in the atmosphere and is ignored here.

The conservation equation for moist entropy in the boundary layer may be written

$$\frac{\partial s_b}{\partial \tau} + \frac{dR}{dt}\frac{\partial s_b}{\partial R} + \frac{1-\sigma}{2}(\omega_{a0} + |\omega_{a0}|)\frac{s_b - s_m}{\Delta P_b} = g\frac{\partial F_s}{\partial P}, \quad (27)$$

where ΔP_b is the pressure depth of the subcloud layer and F_s is the turbulent vertical flux of entropy along R surfaces. The last term on the left-hand side of (27) is the mean flux of entropy through the top of the subcloud layer outside of clouds; it is nonzero only where the motion is downward.

We approximate the right-hand side of (27) by the difference between the sea surface flux of entropy and the convective flux out of the subcloud layer. We therefore write (27) as

$$\frac{\partial s_b}{\partial \tau} + \frac{dR}{dt}\frac{\partial s_b}{\partial R} + \frac{1-\sigma}{2}(\omega_{a0} + |\omega_{a0}|)\frac{s_b - s_m}{\Delta P_b} + \frac{\sigma}{2}(\omega_c + |\omega_c|)\frac{s_b - s_m}{\Delta P_b} = \frac{g\rho_0 C_D |V_b|(s_s^* - s_b)}{\Delta P_b}, \quad (28)$$

where dR/dt is given by (10) and (14) and we have once again used the aerodynamic flux formula for the surface fluxes [with C_D given by (18)]. The term s_s^* is the saturation moist entropy at the ocean surface. The last term on the left is the convective flux and is nonzero only when convective downdrafts enter the subcloud layer; these are assumed to transport entropy (s_m) from the lower model layer. The sea surface saturation entropy can be derived from the definition of moist entropy and may be written in the form

$$s_s^* = s_{bi} - R_d \ln\frac{p}{p_0} + \frac{L_v}{T_s}r_s^*\left(\frac{p_0}{p} - \text{RH}_a\right), \quad (29)$$

where s_{bi} is the initial mean boundary-layer entropy, R_d the gas constant, L_v the latent heat of vaporization, r_s^* and RH_a the ambient boundary-layer saturation mixing ratio and relative humidity, and p_0 is the ambient surface pressure. The above shows that as the surface pressure decreases, the saturation entropy at the ocean surface increases, as noted by Byers (1944) and Riehl (1954). Emanuel (1986) demonstrated that roughly half the heat input into mature hurricanes is due to this effect, assuming that the inflow is approximately isothermal. The derivation of (29) assumes that the atmospheric temperature is always equal to the sea surface temperature.

The conservation equation for total entropy in the lower model layer (s_m) involves mean fluxes through the bottom and top of the layer, convective fluxes due to clouds that detrain in the lower layer, and radiational cooling:

$$\frac{\partial s_m}{\partial \tau} + \frac{1-\sigma}{2}(\omega_{a0} - |\omega_{a0}|)\frac{s_b - s_m}{\Delta P} + \frac{1-\sigma}{2} \times (\omega_a + |\omega_a|)\frac{s_m - s_t}{\Delta P} + \frac{\sigma}{2}(\omega_c - |\omega_c|) \times \frac{s_b - s_m}{\Delta P} = -\frac{\Gamma_m}{\Gamma_d}\,\mathrm{rad}(s_m^* - s_{mi}^*), \quad (30)$$

where s_t is the total entropy of the top layer. As we do not predict s_t, we here assume that it is initially equal to the total entropy that would be obtained by linearly extrapolating the initial entropy distribution to the middle level of the model, and that changes of s_t track changes in s^*:

$$s_t = 2s_{mi} - s_{bi} + s^* - s_i^*. \quad (31)$$

This is nearly equivalent to assuming that the relative humidity of the upper layer remains fixed.

g. *Representation of cumulus convection*

In the formulation of this model, cumulus convection represents sources and sinks of mass [the G term in (9) and (16)] and of entropy [the ω_c terms of (28) and (30)] to the explicitly predicted environment of cumulus clouds. Momentum transport is automatically accounted for in this model since the convection is assumed to redistribute heat on angular momentum (R) surfaces.

The general representation of convective clouds is illustrated in the context of the model structure in Fig. 1. Each "cloud" is, in effect, a representation of the effect of a cloud integrated over its lifetime. The clouds each consist of an updraft–downdraft couplet. The sum of the updraft and downdraft, multiplied by a fractional area covered by the drafts, represents the *net* mass flux which appears in the mass continuity equation. This mass flux drives the circulation outside of the clouds and induces temperature changes through the adiabatic warming by this forced circulation. The updrafts also transport entropy out of the subcloud layer and into either the lower or upper model layers, depending on the depth of the cloud, while the downdrafts transport low entropy air into the subcloud layer.

The updraft mass flux is calculated by integrating the parcel equation for slantwise ascent, based on the buoyancy of subcloud-layer air lifted upward along R surfaces, to obtain a cloud vertical velocity; this is then multiplied by an assumed fractional area to get the mass flux. The downdraft mass flux is taken to be the updraft flux multiplied by $(1 - \epsilon)$, where ϵ is the total precipitation efficiency of the cloud. That is, a nonprecipitating cloud ($\epsilon = 0$) has equal net vertically integrated updraft and downdraft mass fluxes and so produces no *net* heating, while a cloud without any evaporation ($\epsilon = 1$) produces no downdraft.

The precipitation efficiency of each cloud is specified as a function of the cloud depth. In the case of this simple model only two cloud types are represented: deep clouds with a precipitation efficiency of 1, and shallow, nonprecipitating clouds. While the latter have no vertically integrated net mass flux (i.e., there is no net heating over a cloud lifetime), they do exchange total entropy between the subcloud and lower model layers.

The deep and shallow clouds may, and in general do, coexist. In this case, the shallow clouds may be thought of as, to some extent, representing the effect of precipitating downdrafts within the coarse vertical resolution of this model. The two have the same effects because if no evaporation occurs in the upper layer, then there will be no *net* mass source due to precipitating downdrafts below the model's middle level. There will, however, be an exchange of entropy between the subcloud layer and the boundary layer due to cold downdrafts penetrating the boundary layer and a compensating mass flux into the lower model layer. Thus, *in the model, the effects of shallow clouds and of precipitating downdrafts are identical.* In section 3d we describe several experiments in which shallow clouds are replaced by precipitation-induced downdrafts.

The vertical velocity in deep clouds is predicted by first finding the velocity characterizing slantwise ascent. This can be estimated by integrating the slantwise convection parcel equations developed by Emanuel (1983). In cylindrical coordinates, these are

$$\frac{dw}{dt} = B,$$

$$\frac{du}{dt} = f(v - v_g) + \frac{v^2 - v_g^2}{r} = \frac{f^2}{4r^3}(R^4 - R_g^4),$$

where R_g is the potential radius that would be obtained if the flow were in gradient balance, and B is the buoyancy of a parcel lifted adiabatically from the subcloud layer:

$$B = g\frac{\Gamma_m}{\Gamma_d}\frac{1}{c_p}(s_b - s^*). \tag{32}$$

The momentum equations can be combined into an equation for the absolute velocity, U, of slantwise ascent:

$$\frac{1}{2}\frac{d}{dt}(u^2 + w^2) \equiv \frac{1}{2}\frac{d}{dt}U^2 = wB + u\frac{f^2}{4r^3}(R^4 - R_g^4)$$

or

$$\frac{dU}{dt} = B\sin\theta + \frac{f^2}{4r^3}(R^4 - R_g^4)\cos\theta,$$

where θ is the angle a parcel trajectory makes with the horizontal. This in turn may be rewritten

$$\frac{dU}{dt} = B\frac{\partial z}{\partial l} + \frac{f^2}{4r^3}(R^4 - R_g^4)\frac{\partial r}{\partial l},$$

where l is a unit vector along the direction of parcel motion.

Emanuel (1983) showed that the kinetic energy a parcel gains in slantwise ascent is the same regardless of the path the parcel follows, as long as the end-points are the same. For the purposes of estimating this velocity we force the parcel up its original R surface, so that

$$\frac{dU}{dt} = B\left(\frac{\partial z}{\partial l}\right)_R,$$

or in R coordinates,

$$\frac{\partial U}{\partial \tau} + \frac{dR}{dt}\frac{\partial U}{\partial R} + \omega\frac{\partial U}{\partial P} = B\left(\frac{\partial z}{\partial l}\right)_R.$$

Here $(\partial z/\partial l)_R$ is the slope of R surfaces. Making use of the relations $\omega \approx U(\partial p/\partial l)$, and also of (10) and (14), the above may be integrated along an R surface between the sea surface and the middle level to yield

$$\frac{\partial U_s}{\partial \tau} + \frac{rg}{fR}\frac{F_{vs}}{\Delta P}\frac{\partial U_s}{\partial R} + \frac{1}{2}\frac{U_s^2}{\Delta P} = \frac{1}{\Delta P}\int_0^{z_t} B\,dz \equiv \bar{B}\frac{z_t}{\Delta P}. \approx \frac{\bar{B}}{\bar{\rho} g} \tag{33}$$

Here U_s represents the slantwise velocity assumed to be nearly constant and positive between the top of the subcloud layer and the middle level. The reason for using (33) instead of simply setting $U_s^2 = 2Bz_t$ is merely that it results in a smoother numerical integration of the model.

To obtain the vertical component, ω_t, it is necessary to account for the slope of R surfaces:

$$\omega_t = \frac{-\rho g U_s}{\left[1 + \left(\frac{\partial r}{\partial z}\right)_R^2\right]^{1/2}},$$

where $(\partial r/\partial z)_R$ is the slope of R surfaces from the vertical. From the thermal wind equation (Emanuel 1986), we have

$$\frac{1}{r^3}\left(\frac{\partial r}{\partial z}\right)_R = \frac{1}{f^2R^3}\left(\frac{\partial T}{\partial z}\right)_{s^*}\frac{ds^*}{dR} = \frac{1}{2}\frac{\Gamma_m}{T_s - T_t}\left(\frac{1}{r_b^2} - \frac{1}{r_t^2}\right),$$

or

$$\left(\frac{\partial r}{\partial z}\right)_R = \frac{1}{2}\frac{\Gamma_m}{T_s - T_t}r^3\left(\frac{1}{r_b^2} - \frac{1}{r_t^2}\right).$$

If the slope is evaluated at the top of the boundary layer, then

$$\omega_t = \frac{-\rho_0 g U_s}{\left\langle 1 + \left\{\frac{1}{2}\frac{\Gamma_m}{T_s - T_t}r_b\left[1 - \left(\frac{r_b}{r_t}\right)^2\right]\right\}\right\rangle^{1/2}}. \tag{34}$$

Note that where $r_b = r_t$ (R surfaces are vertical), ω_t is just equal to the slantwise mass flux per unit area. When $r_t \gg r_b$, however, and r_b is not small, the vertical velocity is considerably smaller than the slantwise velocity. This effectively increases the time scale of convective adjustment, which in the case of slantwise convection is considerably larger than that for upright convection.

In order to obtain the deep-cloud mass flux it is necessary to multiply ω_t by σ, the fractional convergence of deep clouds. Here we must make an assumption about the distribution of deep convection. Were we using a fixed grid, it is quite likely that the model would be insensitive to the choice of σ simply because, as demonstrated in the next subsection, the time scale of convection is so fast compared to the time scale of evolution of the cyclone that slowing it down or speeding it up even an order of magnitude will not affect the dynamics on the cyclone time scale.

In the model, however, the physical distance between R surfaces can become comparable to the scale of convection, especially around the eyewall of mature model storms. With fixed σ, the actual cumulus mass flux will be made artificially small when this happens. To avoid this, we make the simple assumption that *there can be at most one deep convective cloud per grid volume.* The fractional area covered by deep clouds is then simply the dimension of the cloud divided by the dimension of the grid box. In two dimensions, then, this may be written

$$\sigma_t = \begin{cases} \dfrac{\Delta r_c}{\Delta r_b}, & \dfrac{\Delta r_c}{\Delta r_b} \leq 1 \\ 1, & \dfrac{\Delta r_c}{\Delta r_b} > 1, \end{cases} \tag{35}$$

where Δr_c is a typical width of a deep convective cloud (here taken to be the depth of the model atmosphere) and Δr_b is the distance between adjacent R surfaces, measured at the top of the subcloud layer.

In the case of shallow convection, we assume that the cloud field is always in equilibrium with the environment and, as mentioned before, that each shallow cloud consists of an updraft and downdraft of identical magnitude. Thus

$$\omega_s = \omega_u + \omega_d,$$

with

$$\omega_u^2 = \frac{\Delta P \bar{\rho} B_s g}{1 + \left[\frac{1}{2}\frac{\Gamma_m}{T_s - T_t} r_b \left(1 - \frac{r_b^2}{r_t^2}\right)\right]^2} \tag{36}$$

(for $B_s > 0$), and

$$\omega_d = -\omega_u.$$

Here the buoyancy is

$$B_s = g \frac{\Gamma_m}{\Gamma_d} \frac{1}{c_p} (s_b - s_m^*). \tag{37}$$

We assume that the shallow clouds are always subgrid scale, and take the fractional area of the updrafts and downdrafts to be equal, with the value σ_s.

At first glance, it might seem that (36) yields the result that shallow clouds have no effect. Indeed, they do not appear as mass sources and thus make no contribution to the integrated mass flux given by (6) (i.e., they produce no net heating). However, when the updrafts and downdrafts are entered separately into the entropy budget equations (28 and 30), their effect is finite. All shallow clouds do in this model (and in the real atmosphere) is exchange entropy between the subcloud layer and the free atmosphere at a rate dictated by parcel buoyancy.

h. Scaling appropriate for air–sea interaction systems

It is both convenient and, in this case, very instructive to incorporate as much of the parameter dependence as possible in scaling the dependent and independent variables of the model. The natural scaling in this system revolves around a measure of the thermodynamic disequilibrium between ocean and atmosphere. This measure is defined

$$\chi_s \equiv (T_s - T_t)(s_{s0}^* - s_{bi}), \tag{38}$$

where s_{s0}^* is the saturation entropy at the sea surface at ambient pressure and s_{bi} is the initial (ambient) subcloud-layer entropy. The quantity χ_s has units of kinetic energy per unit mass, and its square root provides a natural velocity scale for hurricanes. We shall see that virtually all the dependence of hurricane intensity on sea surface temperature and tropopause temperature is contained in (38), although some dependence remains in the actual (pressure dependent) saturation entropy of the sea surface.

It is natural to define an entropy variable χ to replace all the moist entropies and saturation moist entropies in the model. Thus we replace all entropies by

$$\chi \equiv (T_s - T_t)(s - s_{bi}), \tag{39}$$

where s here stands for all of the model moist entropy variables [e.g., $\chi_m \equiv (T_s - T_t) \times (s_m - s_{bi})$].

We next scale all the model variables as follows:

$$\begin{aligned}
\chi_b &\to \chi_s[\chi], \\
\chi_m &\to \chi_s[\chi_m], \\
\chi^* &\to \chi_s[\chi^*], \\
\chi_m^* &\to \chi_s[\chi_m^*], \\
r &\to \frac{\sqrt{\chi_s}}{f}[r], \\
R &\to \frac{\sqrt{\chi_s}}{f}[R], \\
\tau &\to C_{D0}^{-1} \frac{R_d T_s}{g} \frac{\Delta P}{p_0} \chi_s^{-1/2}[\tau], \\
V &\to \sqrt{\chi_s}[V], \\
\psi &\to \frac{1}{2} C_{D0} \rho_s g \chi_s^{3/2} f^{-2}[\psi], \\
\omega &\to C_{D0} \rho_s g \chi_s^{1/2}[\omega], \\
p &\to p_0 \left[\exp\left(\frac{\chi_s[P]}{R_d T_s}\right)\right].
\end{aligned} \tag{40}$$

In all of the above, the bracketed quantities are dimensionless. Also, ρ_s is the mean surface-air density, p_0 is the ambient surface pressure, R_d is the gas constant, and g is the acceleration of gravity.

Before summarizing the nondimensional equations, it is worth examining the scaling in more detail, as this is one of the principal results of the present work.

Typical values of the scales for velocity, radius, time, and pressure are given in Table 1. The azimuthal velocity scale depends only on the thermodynamic dis-

TABLE 1. Typical values of the scaling parameters in the tropical atmosphere.

Quantity	Scale	Typical value*
Azimuthal velocity	$\chi_s^{1/2}$	60 m s^{-1}
Radial velocity	$\frac{1}{2}\frac{p_0}{\Delta P}\frac{g}{R_d T_s} C_{D0}\chi_s f^{-1}$	10 m s^{-1}
Vertical velocity	$C_{D0}\chi_s^{1/2}$	6 cm s^{-1}
Radius	$\chi_s^{1/2} f^{-1}$	1000 km
Time	$C_{D0}^{-1}\frac{R_d T_s}{g}\frac{\Delta P}{p_0}\chi_s^{-1/2}$	16 hours
Pressure perturbation	$p_0\left[\exp\left(\frac{\chi_s}{R_d T_s}\right) - 1\right]$	45 mb
θ_e perturbation	$\theta_e^*\left[1 - \exp\left(\frac{-\chi_s}{c_p(T_s - T_t)}\right)\right]$	13 K

*The following parameter values have been used:

$T_s = 27°C$	$p_0 = 1000$ mb
$T_t = -70°C$	$\Delta P = 400$ mb
Ambient surface relative humidity = 80%	$C_{D0} = 10^{-3}$
$f = 5 \times 10^{-5}$ s^{-1} (value at 20° latitude)	$\theta_e^* = 360$ K

equilibrium parameter χ_s, as does the pressure scale. This is consistent with the findings of Emanuel (1986), except that the isothermal expansion effect on entropy has not yet been accounted for. This will appear as an additional dimensionless parameter in the nondimensional equations.

The vertical velocity scale is simply the azimuthal velocity scale multiplied by the surface exchange coefficient. This is the same velocity scale that governs surface fluxes (Betts 1983). The results of the numerical integrations show that typical velocities outside of clouds are about an order of magnitude smaller than this, while cloud mass fluxes are roughly an order of magnitude larger.

The radial velocity scales as the vertical velocity multiplied by the ratio of the radius scale to a depth scale, as expected from continuity.

The radius scale defines an upper bound for the geometric scale of the entire cyclone. This upper bound was discussed by Emanuel (1986) and is determined by the proportion of energy from the Carnot cycle used to spin up the anticyclone aloft. If the outer scale of the cyclone is too large, the frictional dissipation necessary to move air out of the anticyclone is greater than can be supplied by the Carnot cycle and no amplification is possible. (The impossibility of steady-state hurricanes without sources of angular momentum in the outflow was established by Anthes 1974, and is also clear from the Carnot cycle argument of Emanuel 1986.)

As expected, the time scale varies inversely with the surface-exchange coefficient. This can be thought of as an Ekman spindown time scale, i.e., the depth scale divided by the surface-stress scale, $C_{D0}|V| \sim C_{D0}\chi_s^{1/2}$. Alternatively, it may be viewed as the time scale for air to move vertically through the cyclone, i.e., the depth scale divided by the vertical velocity scale. It is also, of course, the spinup time scale for the cyclone and indicates faster spinup for greater air–sea thermodynamic disequilibrium, as found for example by RE (see their Fig. 7).

All of the entropy values scale with χ_s. In the ambient subcloud layer, χ is zero by definition (39). As the tropics are approximately conditionally neutral, $\chi^* \approx \chi = 0$. The middle tropospheric entropy variable χ_m is negative since $s_m < s_b$ (that is, θ_e decreases upward in the lower troposphere). For fixed dimensionless χ_m, the dimensional χ_m (proportional to $s_m - s_b$) becomes more negative for increasing χ_s, implying that the difference between subcloud layer and middle-tropospheric entropy scales with the air–sea thermodynamic disequilibrium.

i. *Summary of dimensionless model equations and parameters*

When the scalings (40) are applied to the model equations (2, 9, 13, 16, 18, 20–24, 26, and 28–37) the following dimensionless set results. All the variables are dimensionless [we have dropped the brackets that appear in (40)]. The dimensionless coefficients that appear are listed in Table 2 and will be discussed after presentation of the equations.

Thermal wind:

$$\frac{1}{r_b^2} = \frac{1}{r_t^2} - \frac{2}{R^3}\frac{\partial \chi^*}{\partial R}. \tag{41}$$

Physical radius at top of model:

$$\frac{\partial r_t^2}{\partial \tau} = \psi - G. \tag{42}$$

Physical radius at top of subcloud layer:

$$\frac{\partial r_b^2}{\partial \tau} = \psi_0 - \psi - \frac{1}{R}\frac{\partial}{\partial R}\left[r_b^3 \nu \frac{\partial}{\partial r_b}\left(\frac{R^2}{r_b^2}\right)\right], \tag{43}$$

with

$$G = \int_0^{r_b^2} \sigma_t \omega_t dr'^2 \tag{44}$$

$$\nu = l^2\left|r_b \frac{\partial}{\partial r_b}\left(\frac{R^2}{r_b^2}\right)\right|. \tag{45}$$

Streamfunction at top of boundary layer:

$$\psi_0 = G + (1 + C|V_b|)|V_b|\frac{1}{2R}\frac{\partial r_b^2}{\partial R}(R^2 - r_b^2) \tag{46}$$

TABLE 2. Nondimensional model parameters.

Parameter	Name	Definition	Typical value
α	Cloud buoyancy parameter	$\frac{\Gamma_m}{\Gamma_d}\frac{\Delta P}{p_0}\frac{R_d T_s}{c_p(T_s - T_t)} C_{D0}^{-2}$	10^5
Q	Dry static stability	$\frac{\Gamma_d}{\Gamma_m} c_p(T_s - T_t)\chi_s^{-1}\left(-\frac{\overline{\partial \ln\theta}}{\partial p}\right)\Delta P \approx \frac{1}{2}\frac{\Gamma_d}{\Gamma_m}\frac{RH_a}{1 - RH_a}$	2
l^2	Eddy mixing scale (squared)	$l_d^2 f^3 \chi_s^{-3/2} C_{D0}^{-1}\frac{R_d T_s}{g}\frac{\Delta P^*}{p_0}$	—
β	Isothermal expansion parameter	$\chi_s / R_d T_s$	0.042
RH_a	Ambient relative humidity	—	0.8
rad	Radiative relaxation rate	$(\mathrm{rad})_d C_{D0}^{-1}\frac{R_d T_s}{g}\frac{\Delta P}{p_0}\chi_s^{-1/2}$**	3
γ	Boundary layer relative depth	$\Delta P_b / \Delta P$	0.1–0.2
C	Wind dependence of surface exchange coefficient	$\frac{C_{D1}}{C_{D0}}\sqrt{\chi_s}$	2
A	Aspect ratio	$\frac{f}{\sqrt{\chi_s}}\frac{\Gamma_d}{\Gamma_m}\frac{c_p(T_s - T_t)}{g}$	0.017

* The dimensional horizontal mixing length is l_d.
** The dimensional radiative relaxation rate is $(\mathrm{rad})_d$.

with

$$V_b = \frac{1}{2}\frac{R^2 - r_b^2}{r_b}. \tag{47}$$

Saturation moist entropy at middle level:

$$\frac{\partial \chi^*}{\partial \tau} = Q(1 - \sigma_t)\omega_a + \frac{\partial}{\partial r_b^2}\left(r_b \nu \frac{\partial \chi^*}{\partial r_b}\right) - \mathrm{rad}(\chi^*), \tag{48}$$

with

$$(1 - \sigma_t)\omega_a = -\frac{\partial \psi}{\partial r_i^2}, \tag{49}$$

and r_m^2 given by

$$\frac{1}{r_i^2} = \left(\frac{T_s - T_m}{T_s - T_t}\right)\frac{1}{r_t^2} + \left(\frac{T_m - T_t}{T_s - T_t}\right)\frac{1}{r_b^2}. \tag{50}$$

[The latter has been formed by combining (26) with (2).] We also impose the restrictions that $\mathrm{rad}(\chi^*) \leq 0.2$ (about 2°C day^{-1}) and that rad = 0 where there is positive Ekman pumping.

Saturation moist entropy in lower layer:

$$\frac{\partial \chi_m^*}{\partial \tau} = Q\left(\frac{\omega_a + \omega_0}{2}\right) - \mathrm{rad}(\chi_m^*) \tag{51}$$

with

$$\omega_0 = -\frac{\partial \psi_0}{\partial r_b^2}. \tag{52}$$

Subcloud-layer moist entropy:

$$\gamma\frac{\partial \chi}{\partial \tau} = \psi_0\frac{\partial \chi}{\partial r_b^2} - \left(\frac{\omega_0 + |\omega_0|}{2}\right)(\chi - \chi_m) - \sigma_s\omega_d(\chi - \chi_m) + (1 + C|V|)|V|(\chi_s^* - \chi), \tag{53}$$

with

$$\chi_s^* = 1 - \frac{T_s - T_t}{T_s}P + \frac{1}{1 - \mathrm{RH}_a}[e^{-\beta P} - 1]. \tag{54}$$

Lower-layer moist entropy:

$$\frac{\partial \chi_m}{\partial \tau} = -\left(\frac{\omega_0 - |\omega_0|}{2}\right)(\chi - \chi_m) + (\omega_a + |\omega_a|) \times (\chi_t - \chi_m) - \sigma_s\omega_u(\chi - \chi_m) - \frac{\Gamma_m}{\Gamma_d}\mathrm{rad}(\chi_m) \tag{55}$$

with

$$\chi_t \equiv 2\chi_{mi} + \chi^*. \tag{56}$$

Deep updraft mass flux:

$$\frac{\partial U_t}{\partial \tau} = \psi_0\frac{\partial U_t}{\partial r_b^2} + \alpha(\chi - \chi^*) - \frac{1}{2}U_t^2, \tag{57}$$

$$\omega_t = \frac{-U_t}{\left\{1 + \left[\frac{1}{2A}r_b\left(1 + \frac{r_b^2}{r_t^2}\right)\right]^2\right\}^{1/2}} \tag{58}$$

with

$$\sigma_t = \frac{A}{\Delta r_b} \quad (\sigma_t \leqslant 1) \tag{59}$$

Shallow updraft and downdraft mass fluxes:

$$\omega_u = -\left\{\frac{\alpha(\chi - \chi_m^*)}{1 + \left[\frac{r_b}{2A}\left(1 + \frac{r_b^2}{r_t^2}\right)\right]^2}\right\}^{1/2} = -\omega_d, \tag{60}$$

with

$$\sigma_s = 0.5. \tag{61}$$

The last relation needed to close the system is a diagnostic equation for the surface pressure variable P. The dimensionless gradient wind relation is

$$\frac{\partial P}{\partial r} = V + \frac{V^2}{r}.$$

It is instructive and numerically beneficial to transform this relation into R coordinates. The above can be shown to be equivalent to

$$\frac{\partial}{\partial R}\left(P + \frac{1}{2}V^2\right) = \frac{R^3}{2r^2} - \frac{R}{2}.$$

By using (41) to eliminate R^3/r^2 on the right of the above, and making use of (47), this can be written as the following relation for surface pressure:

$$\frac{\partial}{\partial R}\left[P + \chi^* + \frac{1}{8}\left(\frac{R^4}{r_b^2} + r_b^2\right)\right] = \frac{1}{2}\frac{R^3}{r_t^2}. \tag{62}$$

The advantage of this form is that in the limit of large r_t (which characterizes the mature stage of the vortex) this can be integrated exactly. Doing this results in an expression for central pressure identical to that obtained by Emanuel (1986).

The system (41)–(62) constitutes the complete set of model equations. The nondimensional parameters that appear in this set are listed in Table 2 and will be described presently.

Of the seven dimensionless parameters, only two are ad hoc: the radiative relaxation rate, rad, and the horizontal mixing scale, l. The motivation for incorporating radiation is the same as in RE, namely, to provide a heat sink to compensate the oceanic source. There are two aspects of the present treatment of radiation that differ from RE. First, we place a cap on the radiative cooling so that it does not exceed about 2°C day^{-1}, as in RE's Experiment J. Second, we turn off the radiative cooling in regions where the Ekman pumping is upward, to mimic crudely the infrared radiative effects of deep clouds over the ocean. As demonstrated in section 4d, the model is somewhat sensitive to the presence of radiative cooling.

The horizontal length scale l is chosen to be quite small, to minimize the artificial diffusion. In order to preserve the scale invariance of the model as much as possible, we let l be proportional to the R spacing of the coordinates. Thus in the control run,

$$l = 0.03\Delta R.$$

In the control run, the dimensional equivalent of l is about 1.5 km, half the value used in RE. As shown in section 3b, the model is remarkably insensitive to l.

The parameter α, which appears in (57) and (60), determines the magnitude of the convective mass fluxes for a given subcloud-layer parcel buoyancy $\chi - \chi^*$. It is the dimensionless multiplier relating vertical acceleration in clouds to cloud buoyancy and can be thought of as the ratio of the large-scale dynamical time scale to a convective time scale. The fact that it is large ($\sim 10^5$) means that χ can never exceed χ^* by very much; i.e., the atmosphere is kept close to neutral equilibrium, as postulated by Arakawa and Schubert (1974). This is evident in all the model simulations discussed in section 3.

The dry static stability parameter Q, appearing in (48) and (51), governs how much warming occurs for a given subsidence rate. The second relationship for Q appearing in Table 2 comes from making the approximation that θ at the tropopause is nearly equal to θ_e in the boundary layer:

$$-\frac{\partial \ln\theta}{\partial p} \approx \frac{\ln\theta_{ea} - \ln\theta_a}{2\Delta P} = \frac{L_v r_s^* \mathrm{RH}_a}{2\Delta P c_p T_s},$$

where θ_{ea} and θ_a are the equivalent and actual potential temperatures in the ambient boundary layer, and r_s^* and RH_a are the ambient saturation mixing ratio and relative humidity. Also, χ_s may be expressed

$$\chi_s = c_p(T_s - T_t)\ln\frac{\theta_{es}}{\theta_{ea}} = \frac{T_s - T_t}{T_s} L_v r_s^*(1 - \mathrm{RH}_a).$$

Substituting these two relations into the definition of Q in Table 2 gives the second relation

$$Q \approx \frac{1}{2}\frac{\Gamma_d}{\Gamma_m}\frac{\mathrm{RH}_a}{1 - \mathrm{RH}_a}.$$

The parameter β appears as a coefficient multiplying pressure in the expression for the sea surface saturation entropy (54). *It is only nondimensional parameter with a significant sea surface temperature dependence* and governs the rate of heat input due to isothermal expansion. All the rest of the dependence on sea surface temperature is contained in the scaling parameter χ_s.

Emanuel (1988b) showed that there is a critical β above which no steady solution for central pressure exists. The minimum sustainable central pressure can be found here by integrating (62) from the center to the radius where $P = 0$ under the assumption of large

r_t and then requiring that $\chi^* = \chi_s^*$ at the storm center. Using (54), this results in the relation

$$P(1-\epsilon) = \frac{1}{4} r_0^2 - \frac{1}{1-\mathrm{RH}_a}(e^{-\beta P} - 1) - 1,$$

where r_0 is the radius at which the pressure perturbation vanishes. It is straightforward to show that this has no solution for sufficiently large β. For the control run to be described in section 3, the critical β is about 0.08.

The parameter γ is the ratio of the pressure depth of the boundary layer to that of the lower main model layer and appears in the boundary-layer entropy equation (53). The fact that it is small implies that the boundary layer is not far from equilibrium, i.e., surface fluxes balance horizontal advection and fluxes out of the top of the boundary layer. As shown in section 3, the model is not sensitive to γ as long as it is small.

The parameter C, which appears in (46) and (53) and which governs the wind dependence of the exchange coefficients, increases with $\sqrt{\chi_s}$. Sensitivity to C will be discussed in section 4c. Finally, A, which appears in (59) and (60), is a measure of the system's aspect ratio: the scale height divided by the radius scale.

j. Boundary and initial conditions and numerical scheme

The numerical scheme integrates the time-dependent dimensionless equations (42), (43), (48), (51), (53), (55), and (57). The streamfunction is derived from a diagnostic equation formed by eliminating the time dependence of (42) and (43) using the thermal wind relation (41) and the saturation moist entropy equation (48). This diagnostic equation is

$$\psi\left(\frac{1}{r_b^4} + \frac{1}{r_t^4}\right) - \frac{2Q}{R^3}\frac{\partial}{\partial R}\left(\frac{\partial \psi}{\partial r_i^2}\right) = \frac{1}{r_b^4}(\psi_0 - D_{r_b}) + \frac{G}{r_t^4} + \frac{2}{R^3}\frac{\partial}{\partial R}(\mathrm{rad}(\chi^*) - D_{\chi^*}), \quad (63)$$

where the "D" terms are the diffusion terms in (43) and (48). The Sawyer–Eliassen equation (63) is elliptic provided $Q > 0$.

The diffusion and radial advection terms require two boundary conditions each on r_b, χ^*, χ, ω_t, and ψ, and a single boundary condition on P. At $R = 0$, symmetry requires that

$$\psi, r_b, \frac{\partial \chi^*}{\partial R}, \frac{\partial \chi}{\partial R}, \frac{\partial \omega_t}{\partial R} = 0 \quad \text{at} \quad R = 0. \quad (64)$$

In order to minimize the effects of an artificial wall placed at some outer radius R_0, we apply an open boundary condition similar to that of Ooyama (1969). To do so, we assume that the flow outside the boundary layer is linear and nondissipative and that no convection occurs at or outside the boundary. Under these approximations, (63) becomes, for $R \geq R_0$,

$$\psi - \frac{Q}{2} R \frac{\partial}{\partial R}\left(\frac{1}{R}\frac{\partial \psi}{\partial R}\right) = G.$$

Since $\partial G/\partial r^2 = \sigma\omega_t = 0$, the above may be written

$$\psi - G - \frac{Q}{2} R \frac{\partial}{\partial R}\left(\frac{1}{R}\frac{\partial}{\partial R}(\psi - G)\right) = 0. \quad (65)$$

The solution for $\psi - G$ from (65) may be expressed in terms of Bessel functions. For the sake of simplicity, we make the approximation that R is large, in which case the solution is simply

$$\psi - G \approx Ae^{-(2/Q)^{1/2}R},$$

where A is a constant. This in turn implies that

$$\frac{\partial}{\partial R}(\psi - G) \approx -\left(\frac{2}{Q}\right)^{1/2}(\psi - G)$$

or

$$\frac{\partial \psi}{\partial R} \approx -\left(\frac{2}{Q}\right)^{1/2}(\psi - G), \quad (66)$$

since $\partial G/\partial R = 0$ when no convection is present. Applying (66) as a boundary condition on ψ at $R = R_0$ matches the interior numerical solution to the exterior, linear analytic solution and guarantees that ψ is well behaved as $R \to \infty$.

The other boundary conditions at $R = R_0$ demand that the radial gradients of χ^* and χ vanish and that the vorticity itself vanishes at $R = R_0$. The latter is not entirely consistent with the condition on ψ, but it is well posed and since it is only used in the diffusion term of (43), which is very small near the boundary, its effect is minimal. Finally, we demand that the pressure perturbation P vanish at $R = R_0$. In summary, the outer boundary conditions are (66) together with

$$\frac{\partial \chi^*}{\partial R}, \frac{\partial \chi}{\partial R}, \frac{\partial}{\partial R}(R^2 - r_b^2), \omega_t, P = 0 \quad \text{on} \quad R = R_0. \quad (67)$$

The numerical solution of (42)–(63) with the boundary conditions (64) and (67) involves straightforward centered differencing and a leapfrog time scheme. A weak time filter of the type employed by Klemp and Wilhelmson (1978) is used to prevent splitting of the solutions. To improve the accuracy of the advection terms in (53) and (57), we calculate r_b, r_t, and G on a staggered grid; i.e., one that is lagged $\frac{1}{2}\Delta R$ from the grid points on which all the other variables are calculated. Note that the advection terms can be written

$$\left(\psi_0 \frac{\partial R}{\partial r_b^2}\right)\frac{\partial}{\partial R}(\chi, \omega_t) \quad (68)$$

and that, from (46), $\psi_0(\partial R/\partial r_b^2)$ is exactly defined at grid points intermediate between those on which χ and

ω_t are defined. As in RE, we use a conservative form of the advection terms; e.g., for the advection of χ,

$$\frac{1}{\overline{r_b}}\left[\overline{r_b\psi_0\frac{\partial R}{\partial r_b^2}\frac{\partial \chi}{\partial R}}\right],$$

where the overbar denotes an average between the two grid points at which r_b is defined.

For purposes of numerical stability, the variables in the diffusion and damping terms are all lagged one time step. Moreover, since the vertical advection and convective flux terms in (53) and (55) all have the mathematical form of damping terms, it is necessary to lag the χ variables in these terms and in the calculation of shallow convection from (59). In the surface entropy flux calculation [the last term in (53)], the wind velocity itself is interpolated to the χ grid points before the flux is calculated.

Finally, the diagnostic streamfunction equation (63) is solved at each time step by a simple overrelaxation technique. This generally converges to the specified accuracy in 1 or 2 iterations, but more iterations are sometimes required at times when new convection is just erupting.

The model integrations begin with no flow in the upper layer and a weak cyclone in the lower layer, similar to the initial condition used by RE. The lower-layer cyclone has the form

$$V=\begin{cases} r_b\dfrac{V_m}{r_m}, & r_b < r_m \\ \dfrac{r_m V_m}{r_b}\left(\dfrac{r_0^2-r_b^2}{r_0^2-r_m^2}\right), & r_m < r_b < r_0 \\ 0, & r_b > r_0, \end{cases}$$

where V_m and r_m are the maximum wind speed and radius of maximum wind, respectively, and r_0 is the radius at which $V = 0$. This represents solid body rotation inside r_m, a Rankine vortex just outside r_m, and a linear decay to zero near r_0. The above may be inverted to find r_b as a function of R using the dimensionless equivalent of (1):

$$r_b^2=\begin{cases} \dfrac{R^2}{1+2(V_m/r_m)}, & R^2 < r_m^2\left(1+2\dfrac{V_m}{r_m}\right) \\ \dfrac{\left(\dfrac{1}{2}R^2-\dfrac{V_m r_m}{1-(r_m/r_0)^2}\right)}{\left(\dfrac{1}{2}-\dfrac{V_m r_m}{r_0^2-r_m^2}\right)}, & r_m^2\left(1+2\dfrac{V_m}{r_m}\right) < R^2 < r_0^2 = R_0^2 \\ R^2, & R^2 > R_0^2. \end{cases} \tag{69}$$

When (69) is calculated on a finite-difference grid, the actual maximum wind and radius of maximum wind will differ slightly from V_m and r_m, respectively.

Having specified the initial vortex, the thermal wind equation (41) is then solved for χ^*. The other variables are initialized as follows:

$$\left.\begin{aligned} \chi &= U_t = 0 \\ \chi_m &= \chi_{mi} \\ \chi_m^* &= \tfrac{1}{2}\chi^* \end{aligned}\right\} \quad \text{at} \quad \tau = 0.$$

The diagnostic relations for ψ_0, ψ, and P are solved at the first time step to yield the initial distributions of those variables.

3. Experiments with and without shallow clouds

In this section we describe the control experiment, several experiments designed to test the sensitivity of the model to various numerical and ad hoc parameters, and an experiment starting from a weak initial vortex. The central experiment described here is a model run with only high-precipitation-efficiency (HPE) clouds; this emphasizes the important role of low-precipitation-efficiency (LPE) clouds in both the genesis and mature phases of the model storms.

a. The control experiment

The parameter values in the control experiment are listed in Table 3. All of the internal parameters have the typical values listed in Table 2 except for the cloud buoyancy parameter, α, which is reduced in order to allow a larger time step. The effects of this reduction are examined in the section 3b.

The model is initialized with a weak warm-core cyclonic vortex in the lower layer, as given by (69), with $r_m = 0.1$, $V_m = 0.3$, and $r_0 = 0.5$. This corresponds to a dimensional radius of maximum winds of about 100 km, maximum wind speed of 18 m s^{-1} and outer radius of 500 km. Bear in mind that since it is not possible to specify the radius of maximum winds and the maximum wind speed independently in an R-coordinate model, those values are approximate. The actual initial radius of maximum winds and maximum wind speed are 0.078 ($\sim$78 km) and 0.22 ($\sim$13 m s^{-1}), respectively, for the control run. These can be compared to the dimensional values for r_m, V_m, and r_0 of 82.5 km, 12 m s^{-1}, and 412.5 km, respectively, used in the control run of RE. The initial lower-tropospheric entropy, -0.5, implies that the difference between the initial entropies of the boundary layer and lower troposphere is half that of the difference between the boundary-layer and sea-surface saturation entropies. For conditions typical of the tropics, this represents a lower-tropospheric θ_e about 6°C less than the boundary layer θ_e, rather less than the mean difference of about 12°C

TABLE 3. Parameters used in the control experiment, A.

Parameter	Name	Value
Internal parameters		
α	Cloudy buoyancy parameter	2×10^4
Q	Dry static stability	2
l	Eddy mixing scale	$0.03\Delta R$
β	Isothermal expansion parameter	0.042
RH_a	Ambient relative humidity	0.8
rad	Radiative relaxation rate	3
γ	Boundary layer relative depth	0.2
C	Wind dependence of exchange coefficient	2
A	Aspect ratio	0.017
Initial conditions		
r_m	Radius of maximum winds	0.1
V_m	Maximum lower-layer wind speed	0.3
r_0	Radius of zero wind	0.5
χ_{mi}	Lower tropospheric entropy	−0.5
Numerical parameters		
NR	Number of R surfaces, including boundaries	24
$d\tau$	Time step	0.004
R_w	Potential radius of outer wall	1.5

in Jordan's (1958) sounding. As shown in section 4b, this promotes earlier growth of the initial disturbance.

The development with time of the maximum wind in the lower layer in the control run (A) is shown by the solid line in Fig. 2. After an initial period of decline, the vortex amplifies into a mature cyclone by $\tau = 7$.

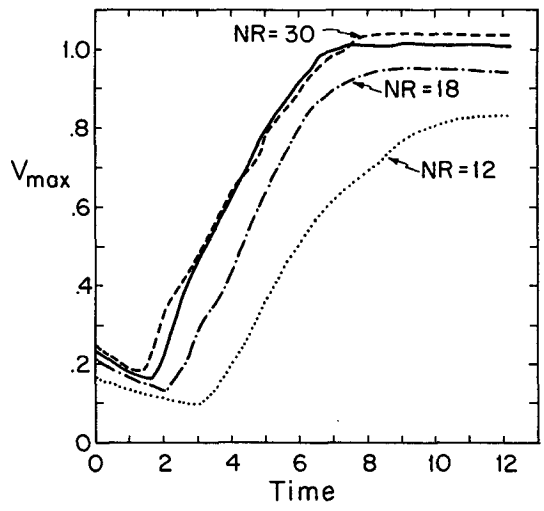

FIG. 2. The maximum dimensionless azimuthal velocity as a function of dimensionless time for the control experiment (solid) and Experiments B_1–B_3 (dashed). Here NR is the number of R-coordinate surfaces in the model, 1 unit of V corresponds to approximately 60 m s^{-1}, and 1 time unit is about 16 h (see Table 1).

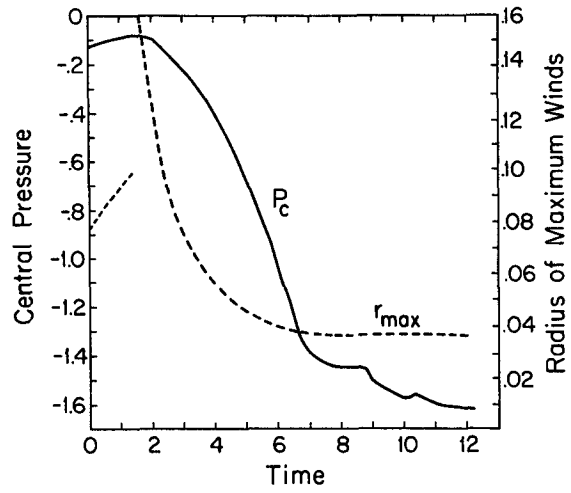

FIG. 3. Evolution with dimensionless time of the dimensionless central pressure (solid) and radius of maximum winds (dashed) in the control run. 1 pressure unit is equal to about 45 mb and 1 radius unit is about 1000 km (see Table 1).

The period of growth starts at about $\tau = 2$, so that the amplification lasts about 5 time units (~80 hours). This is comparable to the development times in the complete model of RE. The time evolutions of the radius of maximum wind and central pressure are shown in Fig. 3. Initially, the radius of maximum wind expands as the vortex weakens. A new ring of maximum winds develops at a larger radius (~0.16 or 160 km) and moves inward to a nearly steady state value of 0.036. The pressure falls to a minimum of about −1.6 (≈ −72 mb) and the most rapid rate of fall is around −0.4 (≈27 mb 24 h^{-1}).

Figure 4 displays the structure of the mature model cyclone in Expt. A at $\tau = 12$. The azimuthal velocity in the lower layer exhibits the classical form, with the velocity peaking at $r = 0.036$ and falling off as $\sim r^{-0.7}$ to about $r = 0.3$ and with a higher negative power of r beyond $r = 0.3$. The radial width of the zone of hurricane force winds ($V \geqslant 0.5$) is about 0.12 (120 km). At the tropopause, there is very weak cyclonic motion out to $r \approx 0.12$ and anticyclonic circulation beyond. The anticyclonic flow has a maximum amplitude of about 0.32 (~19 m s^{-1}) at $r = 0.8$ (~800 km). As there is no frictional dissipation in the upper layer, a front has formed at $r = 0.8$ with nearly infinite cyclonic vorticity (but the circulation is everywhere anticyclonic). This represents the leading edge of the outflow. Although the potential vorticity gradient does not change sign across this front (since the saturated equivalent potential vorticity is zero), the vorticity itself is so large that this zone would likely be unstable to nongeostrophic modes. This evidently happens naturally in three-dimensional models (Anthes 1972b). In any event, this feature is not observed and is almost certainly an artifact of the axisymmetry of the model.

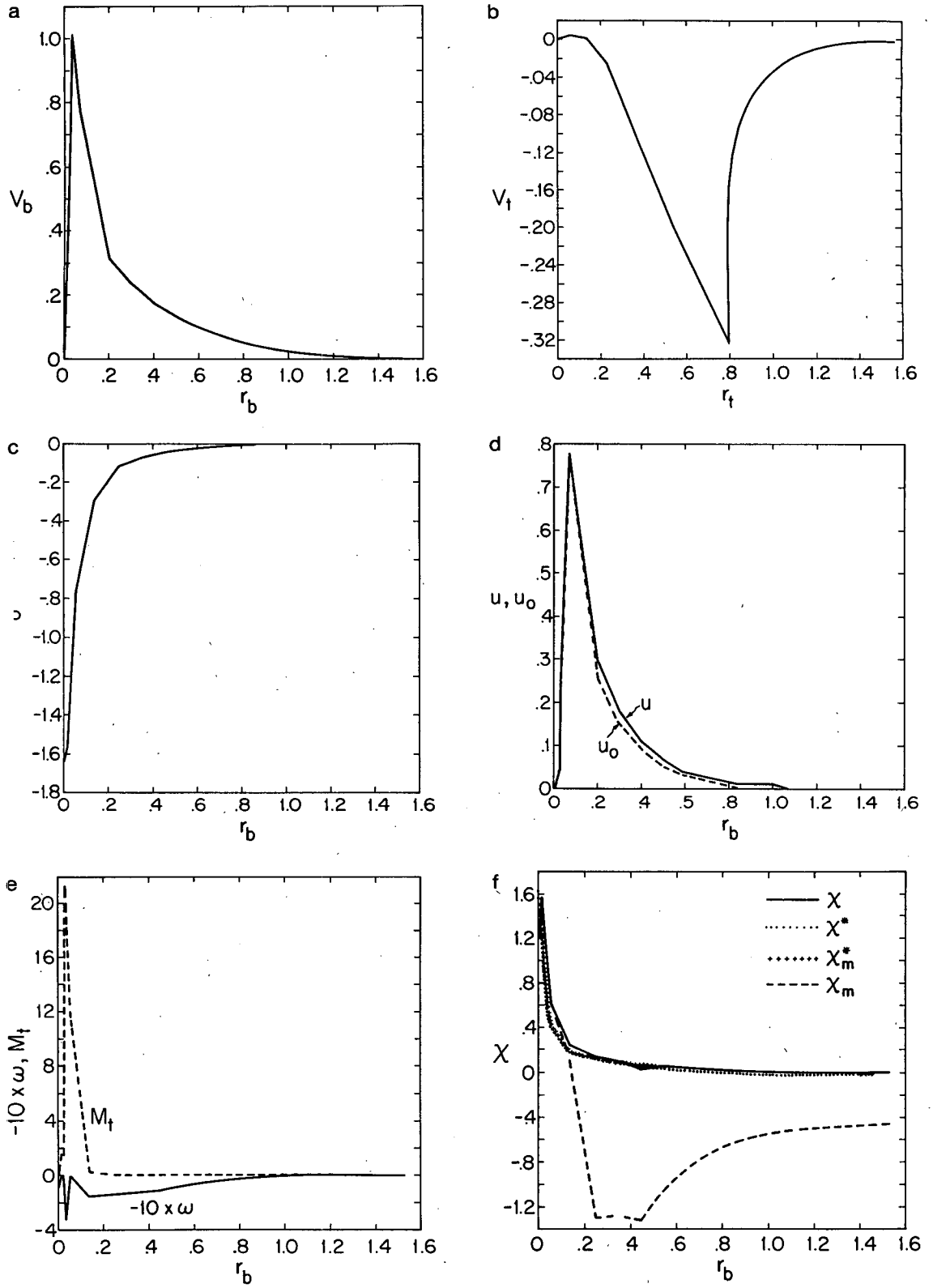

FIG. 4. Structure of the model vortex in the control run at $\tau = 12$. All fields except for V_t are shown as a function of physical radius at the top of the subcloud layer; V_t is plotted against r_t, the physical radius at the top of the model. All variables are dimensionless. (a) Azimuthal velocity at top of subcloud layer; (b) azimuthal velocity at top of model; (c) pressure; (d) negative radial velocity integrated from the surface to the middle level (solid) and to the top of the subcloud layer (dashed); (e) negative omega outside of clouds, multiplied by ten (solid) and deep cloud mass flux ($M_t \equiv -\sigma_t \omega_t$, dashed); (f) subcloud-layer moist entropy (solid), vertically averaged saturation moist entropy (dotted), lower-tropospheric saturation moist entropy (pluses) and lower-tropospheric moist entropy (dashed).

The surface P distribution is relatively uninteresting. The kinks in the distribution reveal the location of R surfaces, which are sparsely spaced in regions of strong anticyclonic relative vorticity. On a surface-pressure map with 4 mb spacing (about 0.1 P units), the outermost closed isobar would occur at $r \approx 0.6$ (600 km).

Figure 4d shows the vertically integrated radial mass flow (u) in the lower half of the model and the vertically integrated frictional flow in the boundary layer (u_b). When the two are equal, all the mass inflow occurs in the boundary layer. Inside $r = 0.2$, u is ever so slightly greater than u_0, mostly to counter the radial momentum diffusion in the near-steady state. Outside $r = 0.2$, $u > u_0$, implying that the vortex is still spinning up in the outer region.

The vertical velocity outside of clouds (Fig. 4e) shows weak subsidence (about 0.15 vertical velocity units, ≈ 1 cm s^{-1}) between $r \approx 0.15$ and $r \approx 0.43$, decaying gradually to zero by $r \approx 1.0$. A sharp spike of downward motion between clouds occurs near the radius of maximum wind, though it is not strong enough to make the net velocity positive. Very weak net subsidence occurs in the eye at this time. The deep cloud vertical mass flux ($\sigma\omega_t$) commences at about $r = 0.25$ but does not become substantial until $r \leq 0.14$, reaching a peak just inside the radius of maximum winds (the azimuthal wind peaks at $r = 0.036$ while the vertical mass flux peaks at $r = 0.032$). The maximum in-cloud vertical velocity multiplied by σ is about 21, corresponding to a dimensional $\sigma\omega$ of about 1.3 m s^{-1}. As $\sigma = 1$ in this run at the location of maximum $\sigma\omega$, this represents the actual cloud vertical velocity there.

All of the moist entropy and saturation moist entropy variables are displayed in Fig. 4f. Outside of $r \approx 0.3$, the atmosphere is slantwise neutral ($\chi \approx \chi^*$) and the lower-troposphere entropy (χ_m) has decreased due to radiation and downward advection of lower χ values. This is consistent with the complete model results of RE, which show a distinct lower-tropospheric θ_e minimum centered near 250 km. Between $r \approx 0.05$ and $r = 0.3$ there is small slantwise instability ($\chi > \chi^*$). Here the R surfaces have a particularly small slope with respect to the horizontal, and the vertical component of the slantwise convective velocity is thus quite small with correspondingly large convective adjustment times. Thus the deep convective cells are too slow to perform a nearly perfect adjustment to neutrality. Even so, the maximum difference between χ and χ^* is about 0.15, corresponding to a buoyancy on the order of 1°C. Thus the model's convection conforms almost exactly to the quasi-equilibrium postulate of Arakawa and Schubert (1974).

While the temperature (saturation moist entropy, χ^*) peaks at the storm center, the boundary-layer and lower-layer moist entropies actual fall slightly in the eye, indicating subsaturation. This is due to subsidence in the eye.

b. Sensitivity to numerical and ad-hoc parameters

We performed a series of experiments in order to examine the model's sensitivity to numerical and ad hoc parameters. All of the additional experiments are listed in Table 4. Experiments B_1–B_3 demonstrate the model's sensitivity to horizontal resolution (in potential-radius space), while C_1–C_3 show how the model behaves when the diffusion is varied. Although the cloud buoyancy parameter, α, is not really an ad hoc parameter (its definition Table 2 is based on strictly physical parameters), we also examine the model's sensitivity to it, as we have elected to use an artificially small α. This sensitivity is explored in experiments D_1 and D_2.

The maximum azimuthal wind is shown as a function of time for experiments B_1–B_3 in Fig. 2. In B_1 only $12R$ surfaces are used and two of these are boundary surfaces. Because of the interpolation onto R surfaces of the initial vortex, B_1 begins with a somewhat weaker vortex. When it does amplify, it does so more slowly and reaches a maximum V that is about 83% of that of the control run. Experiment B_2, with $18R$ surfaces, also begins with a slightly weaker vortex, but it amplifies at almost the same rate as the control, achieving 94% of the latter's amplitude. When $30R$ surfaces are used (B_3), the initial vortex is slightly stronger and amplification begins sooner. The final amplitude is only 2% larger than that of the control experiment.

As mentioned earlier, some radial diffusion is necessary to prevent frontal-like collapse in the eyewall of the model storm. A crude deformation-based mixing

TABLE 4. Description of experiments.

Experiment	Difference from control experiment
A	—
B_1	$NR = 12$
B_2	$NR = 18$
B_3	$NR = 30$
C_1	$l = 0.1\Delta R$
C_2	$l = 0.01\Delta R$
C_3	No momentum diffusion
D_1	$\alpha = 8.0$
D_2	$\alpha = 0.5$
E	$V_m = 0.05$
F_1	No shallow convection
F_2	Same as F_1 but $V_m = 0.05$
F_3	Rainy downdrafts replace shallow convection
F_4	Same as F_3 but $V_m = 0.05$
G_1	$r_m = 0.05$, $r_0 = 0.25$
G_2	$r_m = 0.2$, $r_0 = 1.0$
G_3	$r_m = 0.4$, $r_0 = 1.2$
H_1	$\chi_{mi} = -1.0$
H_2	$\chi_{mi} = -0.25$
I	$C = 0$
J	rad = 0
K	$\gamma = 0.1$
L_1	$\beta = 0.08$
L_2	$\beta = 0.12$
L_3	$\beta = 0.16$

is added to the model to prevent this from happening, but such a formulation is far from realistic. We would therefore hope that the model is relatively insensitive to the value of the assumed mixing length l. Experiments C_1 and C_2 explore this sensitivity (Fig. 5). In C_1, the mixing length is increased by $\sqrt{10}$, so that the effective dissipation rate is an order of magnitude larger. While the initial development is similar, the vortex reaches about 93% of the amplitude of the control. When the dissipation is decreased by an order of magnitude (C_2), the development is almost identical to the control up to $\tau = 3$, but, curiously, is slower between $\tau = 3$ and $\tau = 9$, though the same amplitude is ultimately achieved.

To investigate further the effects of reduced diffusion, we performed an additional experiment, C_3, that is identical to the control run except that radial diffusion of momentum only is turned off. This shows (Fig. 5) that after $\tau = 3$, very little amplification occurs without radial momentum diffusion. Inspection of the velocity and entropy fields shows that the vorticity at the eyewall becomes very large and the radial velocity drops rapidly near the eyewall, presumably due to its inertial stiffness. The inability of the model cyclone to form a realistic eye when momentum diffusion is absent suggests that the dynamics of eye formation are crucial in achieving an intense vortex, as speculated by Malkus (1958). According to the latter and to Kuo (1958; see also Anthes 1974), subsidence in the eye of mature storms is driven by turbulent diffusion of momentum from the eyewall. The subsidence is a dynamic consequence of the differential spinup of the eye between the top and bottom of the storm. Without diffusion, the eye

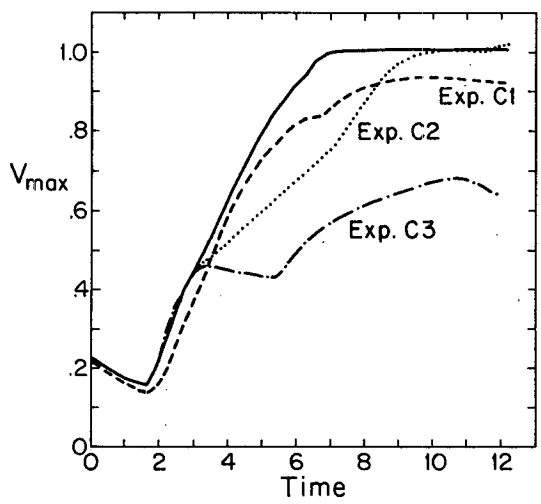

FIG. 5. Evolution with time of maximum azimuthal velocity for control run (solid), and Experiments C_1–C_3. In C_1 the radial diffusion coefficient is increased by one order of magnitude, while in C_2 it is reduced by an order of magnitude. In C_3 there is no radial momentum diffusion.

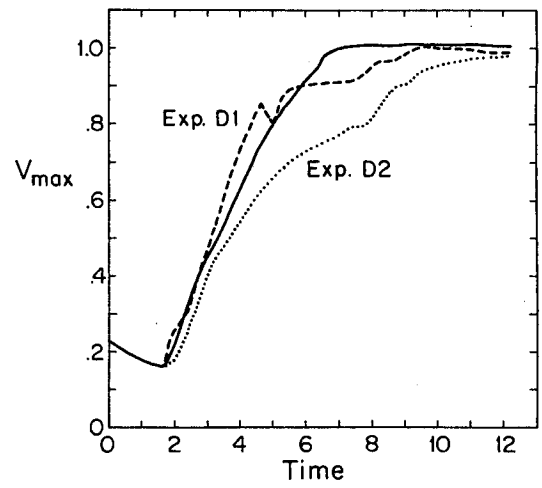

FIG. 6. As in Fig. 5 but for Experiments D_1 and D_2, in which the cloud buoyancy parameter α is increased to 8 and reduced to 0.5, respectively.

remains nearly motionless and may even acquire very weak anticyclonic rotation in the lower region as a result of inflow into the eyewall. Frontogenesis occurs at the eyewall, which cannot contract due to the extreme vorticity (inertial stiffness) of the region just inside the eyewall.

We conclude, in accordance with Malkus (1958) and Kuo (1958), that some radial diffusion is crucial to the development of intense vortices. Even so, the evolution of the vortex is not particularly sensitive to the magnitude of the diffusion, as long as it is not extremely small.

The parameter α relates the convective mass flux to the buoyancy of subcloud-layer air lifted along R surfaces through the depth of the model atmosphere. Although it is a physical parameter, we have reduced it from the nominal value listed in Table 2 to allow a larger integration time step. Experiments D_1 and D_2 (Fig. 6) demonstrate the model's sensitivity to α. In these two experiments, α has been increased and decreased, respectively, by a factor of 4. Clearly, the magnitude of α affects the rate of development of the vortex, but does not seem to influence its ultimate amplitude.

c. Evolution from a weak initial vortex

The main finding of RE, using a complete axisymmetric model, was that weak cyclonic disturbances in convectively adjusted atmospheres do not intensify, implying that tropical cyclones do not arise as a linear instability of the normal tropical atmosphere. This is also the case for the present, simplified model, as illustrated by Experiment E (Fig. 7), which is identical to the control experiment except that the amplitude of the initial vortex is 0.05. Inspection of the saturation moist entropy and moist entropy fields reveals that the

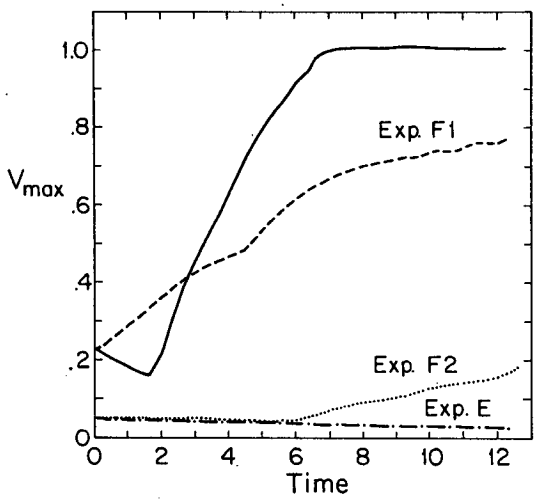

FIG. 7. As in Fig. 5 but for Experiments E, F_1, and F_2. In Experiment E the maximum velocity of the initial vortex is 0.05. In Experiments F_1 and F_2, shallow clouds are turned off; F_1 starts with an amplitude of 0.22, while F_2 begins with $V_{max} = 0.05$.

lower vortex core has become cold and the boundary-layer moist entropy has decreased near the center. The reasons for this behavior will be explored presently.

d. *Experiments without shallow convection*

The evolution of the maximum azimuthal velocity is shown in Fig. 7 for two experiments in which shallow convection is omitted. The convection that does occur has a precipitation efficiency of unity and thus does not account for precipitating downdrafts. Experiment F_1 differs from the control only in this respect, while F_2 is identical to F_1 except that the amplitude of the initial vortex is 0.05, as in Experiment E.

In both cases, intensification occurs immediately, although it is initially very small in Experiment F_2. Note, however, that both the rate of intensification after $\tau = 2$ and the amplitude at $\tau = 12$ are *smaller* in F_1 than in the control. This clearly shows the dual nature of the effect of shallow convection on the model cyclone.

The influence of LPE convection, reflected in Fig. 7, lies at the heart of the thesis of this work. Examination of the various fields reveals the reason for the finite-amplitude behavior of the model cyclones, which may be described as follows.

When a weak vortex is placed in contact with the sea surface, Ekman pumping ensues near the core. The dynamics of the Ekman flow in a stratified fluid are such that the upward velocity reaches a maximum at the top of the boundary layer and decays upward at a rate proportional to the Rossby depth fL/N, where L is a measure of the horizontal dimensions of the vortex, f is the Coriolis parameter, and N is the buoyancy frequency. Thus, *the adiabatic cooling peaks near the top of the boundary layer and decays upward on a Rossby scale.* The conditional instability generated by this cooling very much favors the development of shallow clouds with low (in this case, zero) precipitation efficiency near the core. The shallow, LPE clouds are incapable of countering the adiabatic cooling, but they keep the atmosphere very nearly conditionally neutral by drying out the subcloud layer. Some deep, HPE convection does occur, but peaks outside the radius of maximum winds in a region where the surface fluxes are destabilizing the atmospheric column but the Ekman pumping is weak or negative. The radial motions associated with such convection act to weaken the vortex.

In the case of a stronger initial cyclone, such as in the control run, the same process occurs initially, but after some time the lower troposphere has been moistened by both the Ekman pumping and the shallow, LPE clouds to the extent that the downdrafts are no longer sufficient to counter the moistening of the subcloud layer by evaporation. *When the lower troposphere is sufficiently moist, the downdrafts can no longer counter the moistening of the subcloud layer by surface fluxes, deep, HPE convection breaks out in the core, and intensification begins.*

We emphasize that the important break on initial development is the activity of low-precipitation-efficiency convection, which imports low θ_e air into the boundary layer. This can be accomplished by deep, precipitating convection in which some of the rain evaporates as it falls, as well as by shallow convection. To demonstrate this, we replaced the shallow cloud mass flux given by (60) and (61) by

$$\frac{\partial \sigma_s \omega_u}{\partial \tau} = 10.0(\sigma_t \omega_t - 0.5\sigma_s \omega_u),$$

and

$$\sigma_s \omega_d = -\sigma_s \omega_u.$$

The intent here is to crudely mimic the effect of precipitation-induced downdrafts. According to this formulation, downdrafts form as a result of deep convective updrafts and decay back to zero on a time scale of several hours. If the updraft were to reach a steady state, the associated downdraft mass flux would be somewhat stronger, in accordance with the observation that thunderstorms produce net divergence at the surface. Recall that in the crude structure of the present model, precipitating downdrafts enter the equations exactly as do shallow clouds so that we can represent them in terms of ω_u and ω_d.

The evolution of the maximum azimuthal wind in the experiments with precipitation-driven downdrafts and without shallow clouds is shown in Fig. 8. Here,

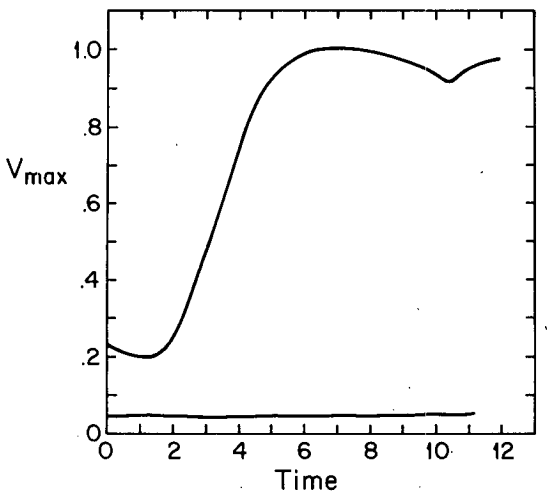

FIG. 8. Evolution of the maximum azimuthal velocity with time for Experiments F_3 and F_4, which omit shallow convection but which contain a crude representation of precipitation-driven downdrafts. Here F_3 and F_4 differ only in their initial amplitudes.

again, the finite-amplitude nature of the instability is apparent, although the simulation beginning with the weaker vortex does not decay but rather fails to amplify (as in RE). Examination of the model fields shows that very weak, deep, LPE convection occurs more or less randomly in space and time outside of the eyewall; the resulting downdrafts keep the subcloud layer cool and dry. Only in the vicinity of the eyewall of the amplifying cyclone, where the atmosphere is nearly saturated, do these downdrafts fail to prevent the surface fluxes from increasing θ_e in the subcloud layer.

This limiting mechanism, which is transparent in the present simplified model, is also consistent with deductions made by RE in the course of examining the complete model fields. Describing the failure of a weak initial vortex to amplify, RE conclude that "owing to the low velocity, latent-heat transfer is slow and cumulus convection does not start until ~70 h. After this time, there is convection, but the cool, dry downdrafts extinguish the instability before the vortex can build up enough speed to increase significantly the sea-surface transfer." The θ_e budget presented by RE shows that time-mean surface fluxes are nearly balanced by convective downdrafts outside the eyewall; near the latter, surface fluxes are more nearly balanced by horizontal advection. Emanuel (1986) showed that steady-state hurricanes would not be possible without a mechanism for keeping the outer subcloud-layer θ_e relatively small.

It is interesting to contrast the results of RE and the present work with CISK theory. As defined by Charney and Eliassen (1964), CISK is a linear instability that does not require the entropy of the boundary layer to increase and as such must depend energetically on ambient conditional instability. In the formulation employed by Charney and Eliassen (1964) and subsequently in many other analytical treatments, the rate of heating is related to low-level or vertically integrated moisture convergence. Since the vertical profile of the heating is specified, the model's temperature is not constrained to relax back to a state of convective neutrality and is therefore inconsistent with observations and convection-resolving nonhydrostatic models such as that of RE. Moreover, the formulation of the entropy budget does not permit downdrafts to actually lower the subcloud-layer entropy beneath ambient values, as observed in RE and in real thunderstorms. We do not see any basis in complete numerical models, in the present model, or in nature for regarding tropical cyclones as arising from the "cooperation of cumulus clouds."

We maintain that the *direct* effect of convective overturning of less than 100% precipitation efficiency is always to lower the subcloud-layer entropy, as is patently obvious in the case of convection over land. The best that purely advective effects (such as moisture convergence) can do is to restore partially the subcloud entropy to its ambient value. Without surface fluxes or radiative effects, convection can do no more than partially damp temperature perturbations arising from other sources.

In view of the preceeding, it is clear that Ekman pumping, by itself, has a damping effect on the cyclone. Only when surface evaporation is sufficient to counter the drying of the boundary layer by the Ekman pumping-induced LPE clouds can the cyclone amplify. Even without Ekman pumping, the cyclone will not intensify until the middle troposphere becomes sufficiently humid that LPE clouds will not completely counter the moistening of the boundary layer by surface fluxes.

e. Comparison with Ooyama's model

The main differences between the present model and that of Ooyama (1969) are the coordinate system, the representation of convection, and the initial condition. The latter two, taken together, lead to an account of hurricane dynamics quite different from Ooyama's description.

The primary effect of the potential-radius coordinate used here is to reduce greatly the number of radial coordinate surfaces necessary to accurately simulate the balanced flow. Whereas Ooyama used 200 coordinate surfaces over 1000 km, we use 24 over 1500 km. Nevertheless, this model's maximum radial resolution, which occurs near the eyewall, is comparable to the uniform 5-km resolution in Ooyama's model. On the other hand, our use of a uniform time step requires about 7 times as many time steps over a roughly 10-day period as required by Ooyama's model, which adjusts the time step during the integration. A

secondary effect of the use of potential-radius coordinates is that the convective adjustment occurs along angular-momentum surfaces, thereby accounting for the centrifugal as well as buoyant component of convection, and for the vertical transport of angular momentum.

The representation of convection used by Ooyama is quite similar to that suggested by Kuo (1965), which is employed in many research and operational numerical models. In simple terms, the rate of heating is proportional to both the difference between the temperature of a parcel lifted from the boundary layer and that of the free atmosphere, and the rate of moisture convergence in the boundary layer. (In Kuo's scheme, some of the moisture converged may be used to moisten, rather than heat, the atmosphere.) This constraint means that *convection is forbidden in regions of moisture divergence.* Consequently, large conditional instability can and does occur outside the core in Ooyama's simulations.

We regard the constraint imposed by moisture convergence as entirely artificial and counter to parcel theory. Although moisture convergence and deep convection are extremely well correlated in the tropics, the former is an *effect* of convection, not its cause. Convection is caused by instability. The effect of the moisture convergence constraint in Ooyama's model is to concentrate high-precipitation-efficiency convection in the core, for reasons very different from those in the present model. In the latter case, the concentration of heating in the core occurs because the precipitation efficiency is very high there, whereas the convection that can and does occur outside the eyewall has relatively low precipitation efficiency.

In effect, the similarity of Ooyama's results and those presented here is due to the spatial near-coincidence of moisture convergence and HPE convection. This coincidence is at least partially accidental, however. In the present model, for example, the moisture convergence that occurs initially is used to moisten, rather than heat the free atmosphere, and deep convection occurs only where surface fluxes are strong enough to generate parcel instability through a deep layer.

Finally, we note that the initial condition used in Ooyama's model is quite unstable to parcel displacements from the boundary layer. (This is not an inherent feature of the model but rather the particular choice made by Ooyama 1969.) A parcel lifted to the middle level acquires approximately 10°C of buoyancy. Consequently, the model is linearly unstable to infinitesimal perturbations. The relatively long incubation time for disturbances was shown by Ooyama to be an artifact of the eddy viscosity in the model. By contrast, the initial state of the present model is conditionally neutral (actually, slightly stable due to the imposition of a weak warm-core vortex) and the initial vortex decays due to boundary friction in the absence of strong heating. As shown in Fig. 5, the present model is relatively insensitive to the magnitude of the lateral eddy viscosity.

4. Other sensitivity experiments

a. Sensitivity to initial vortex dimensions

It is by now well known that tropical cyclones attain a wide range of geometric sizes, and that their intensity is not systematically related to their size (Merrill 1984). The steady-state Carnot-cycle theory of Emanuel (1986) shows that the minimum central pressure that can be sustained in a tropical cyclone is not a strong function of its size up to a large-scale limit, which, using the present normalizations, is given by $r_0 \sim 1$. In terms of the Carnot cycle, too much energy must be used to restore the angular momentum of the outflow to ambient values in a steady-state flow to permit such large sizes. In the model of RE, the cyclonic intensity appeared to be unrelated to its size unless the initial disturbance was too large, in which case it did not amplify. Emanuel and Rotunno (1989) suggest that when the initial disturbance is large, too much energy is used to spin up the anticyclone aloft, which has no feedback on the surface fluxes.

We have performed several experiments designed to determine the sensitivity of the model cyclones to the geometric size of the initial vortex. Figures 9a and 9b show, respectively, the evolution of the maximum azimuthal wind velocity and radius of maximum winds in Experiments G_1–G_3 for which the initial vortex geometry is as listed in Table 4.

In Experiment G_1, the initial vortex geometries are halved. As shown by Fig. 9b, the vortex amplifies by a series of contracting eyewalls, with each successive eyewall attaining an ultimate radius larger than that of its predecessor. Ultimately, the vortex achieves the same dimensions and intensity as in the control run.

Doubling the length scales of the initial vortex (Experiment G_2) leads to a slower intensification (Fig. 9a) but ultimately to a model cyclone that has roughly the same maximum winds as in the control but with somewhat larger dimensions. Quadrupling the initial radius of maximum winds (Experiment G_3), however, greatly slows the intensification rate, as shown in Fig. 9. Examination of the azimuthal velocity at the tropopause (not shown) reveals that the anticyclone is almost as strong as the low-level cyclone in this case, so that less of the total energy feeds back to the surface fluxes.

b. Sensitivity to initial lower-tropospheric humidity

Experiments H_1 and H_2 are designed to test the sensitivity of the model cyclone development to the initial humidity of the lower troposphere above the boundary layer. In the former, the initial entropy difference between the subcloud layer and the lower troposphere is doubled, while in the latter case it is halved. Figure 10

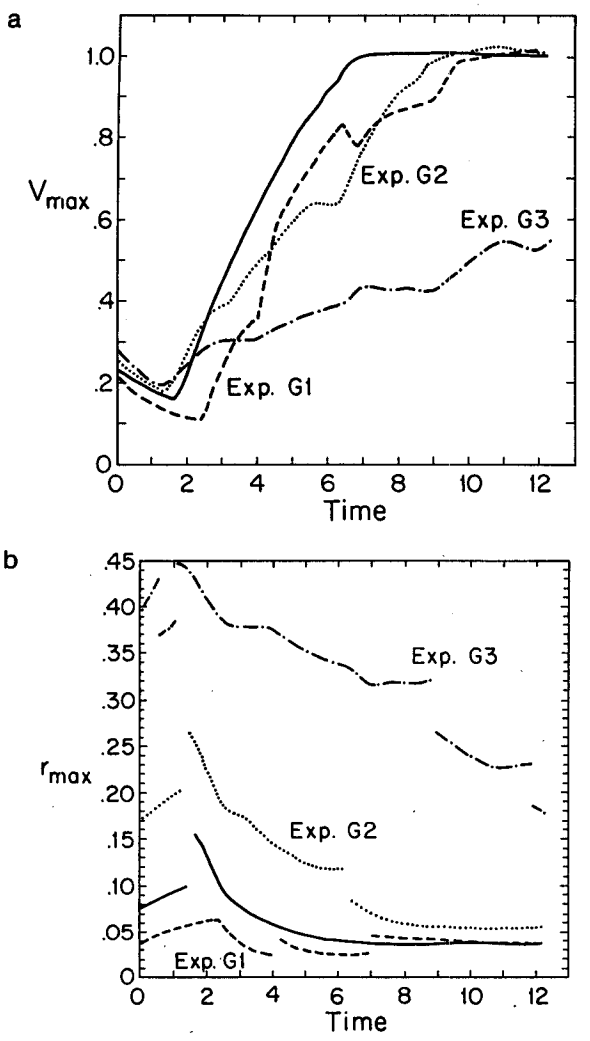

FIG. 9. (a) Evolution with time of maximum azimuthal velocity for control run (solid) and Experiments G_1–G_3. In G_1 the radial dimensions of the initial vortex are halved while in G_2 and G_3 they are doubled and quadrupled, respectively. (b) As in Fig. 9a but showing evolution of radii of maximum winds.

shows that once intensification has begun, the rate of amplification does not vary much with initial lower-tropospheric entropy. The time of onset of intensification, however, is doubled in the first case and halved in the second, suggesting a direct relationship between the time of onset of amplification and the initial entropy difference between the subcloud layer and lower troposphere. This also suggests that the critical amplitude necessary for growth increases with decreasing lower-tropospheric humidity, though no experiments were carried out to test this idea directly. These results are in good agreement with those from the complete model study of RE and in accord with the observation that a moist lower and middle troposphere is conducive to tropical cyclogenesis.

c. *Sensitivity to exchange coefficients*

While it is generally conceded that the surface-exchange coefficients for heat, moisture, and momentum increase with wind speed, due to increasing roughness of the ocean surface, it is not known what form the increase takes or whether the exchange coefficient for entropy increases at the same rate as that for momentum. Advances in this regard await better measurements of surface fluxes in highly disturbed weather. Sensitivity to this wind dependence is evident in Fig. 11, which compares the control run to Experiment I, in which the wind dependence of the exchange coefficients is eliminated. In the latter case the onset of amplification is delayed, intensification is slower and the amplitude achieved is about 10% smaller than that of the control run vortex. We do not, however, find the drastic increase in the time scale mentioned by RE.

d. *Sensitivity to radiational cooling*

Since the tropical oceans act as a heat source for tropical cyclones, a heat sink is also necessary in a closed system if a truly steady state is to be achieved. This point was stressed by Riehl (1954) in his analysis of the hurricane heat engine. In real tropical cyclones, some of the heat may be exported by nonaxisymmetric motions. Even in a closed system, however, the concentration of high winds and surface fluxes in a relatively small region means that the rate of radiational cooling need increase only a few percent over a 1000-km domain to balance the excess transfer of heat from the ocean.

In the present model, and perhaps in nature, the radiative cooling not only permits a balance in the en-

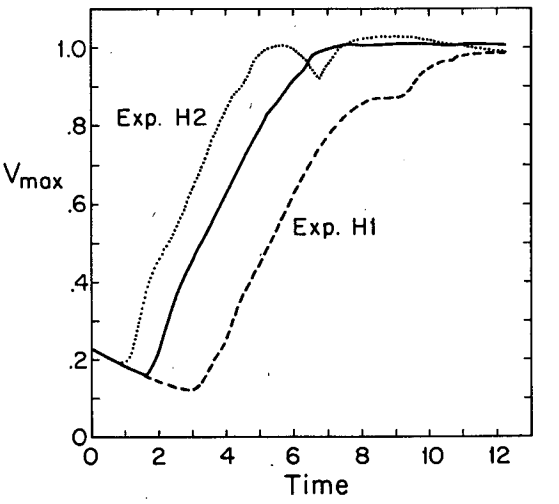

FIG. 10. Evolution with time of maximum azimuthal velocity for control run (solid) and Experiments H_1 and H_2. Here H_1 begins with a very dry middle troposphere while H_2 starts with a relatively moist troposphere.

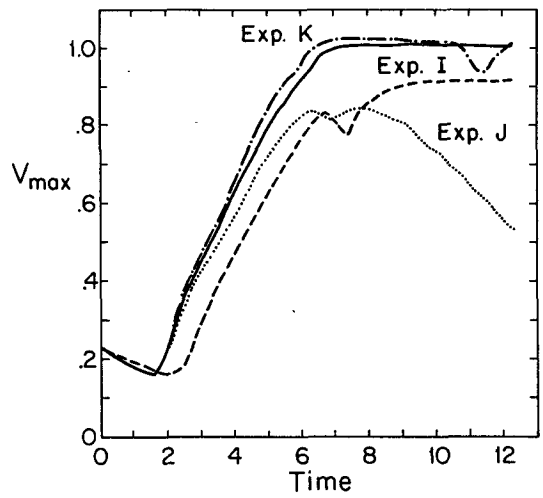

FIG. 11. As in Fig. 10 but for Experiments I, J, and K. In Experiment I the wind dependence of the surface exchange coefficients is eliminated. Experiment J contains no radiative cooling. In Experiment K the subcloud-layer thickness is halved.

ergy equation but also allows subsidence to occur in the steady state. This is important in the moisture budget, since the only way to balance the moistening of the lower troposphere by LPE convection in the hurricane's outer region is by downward advection of dry air.

Figure 11 shows the results of Experiment J, in which radiative cooling is omitted. While the initial evolution is similar to that of the control, the maximum winds attained are only 85% of those of the control, and the vortex decays after about $\tau = 8$. Inspection of the vortex structure reveals that HPE convection occurs in the relatively moist atmosphere outside the eyewall after about $\tau = 6$, and thereafter leads to an expansion and weakening of the wind field. Clearly, the weakening is not so much due to a general warming of the system (which is hardly noticeable at $\tau = 10$) as to the moistening of the lower troposphere outside the radius of maximum winds in the absence of subsidence and the concomitant eruption of HPE convection in the outer region. In reality, this might be prevented by horizontal eddy importation of dry air as well as by radiative cooling. The inward advection of dry air in middle levels is often seen on water vapor channel images from satellites.

e. Sensitivity to subcloud-layer depth

One experiment (Experiment K) was performed in which the depth of the subcloud layer is halved. The results (Fig. 11) show hardly any effect on the evolution of the system. This dramatically illustrates the point that the subcloud layer is always near equilibrium, i.e., that the surface fluxes always balance the sum of horizontal advection and mean and turbulent (convective) fluxes out of the top of the subcloud layer. From a scaling perspective we could omit the time derivative in the subcloud-layer entropy equation and the results show that this would make virtually no difference to the system. Because of horizontal advection, however, it is numerically expedient to retain the time derivative, as we have here.

f. Sensitivity to the isothermal expansion parameter

As mentioned previously, all of the dependence of the model on sea-surface and tropopause temperature is absorbed in the nondimensionalization, save the former's effect on the heat input from isothermal expansion of inflowing subcloud-layer air, as reflected in the nondimensional parameter β (see Table 2).

The evolution of the central pressure with time is illustrated in Fig. 12 for the control experiment and for Experiments L_1–L_3, in which β is increased to 0.08, 0.12, and 0.16, respectively. (Recall that P is proportional to the logarithm of the actual pressure.) As mentioned in section 2i, no steady-state analytic solution exists for sufficiently high β. Without internal dissipation and neglecting the work done to spin up the outflow, this critical value is about 0.08. In the two cases presented here in which β is greater than this value, the central pressure appears to continue falling with time. The integration becomes unstable at about $\tau = 11$ in the case that $\beta = 0.16$, so the integration is stopped at that time. As β increases, the radius of maximum winds in mature cyclones decreases, and inspection of the various fields indicates that radial resolution becomes an increasing problem in spite of the use of potential-radius coordinates.

Variations of β up to about 0.08 cause relatively modest changes in the model cyclone amplitude and structure. Doubling β from 0.042 to 0.08 causes about a 35% decrease in the central pressure and a 15% increase in maximum winds. By contrast, the increase in the scaling factors associated with such an increase in β would double the dimensional pressure drop and increase dimensional wind speeds by 40%.

5. Conclusions

The principal motivation for developing the simple model presented here was to explain in simple terms the finite-amplitude nature of the instability mechanism responsible for tropical cyclones, as portrayed by "complete" nonhydrostatic axisymmetric models such as that of RE. The main difference between the simple model discussed here an other simple models, such as that of Ooyama (1969), is the use of a convective representation that is consistent with parcel instability and which allows for low-precipitation-efficiency (LPE) clouds as well as for deep, high-precipitation-efficiency

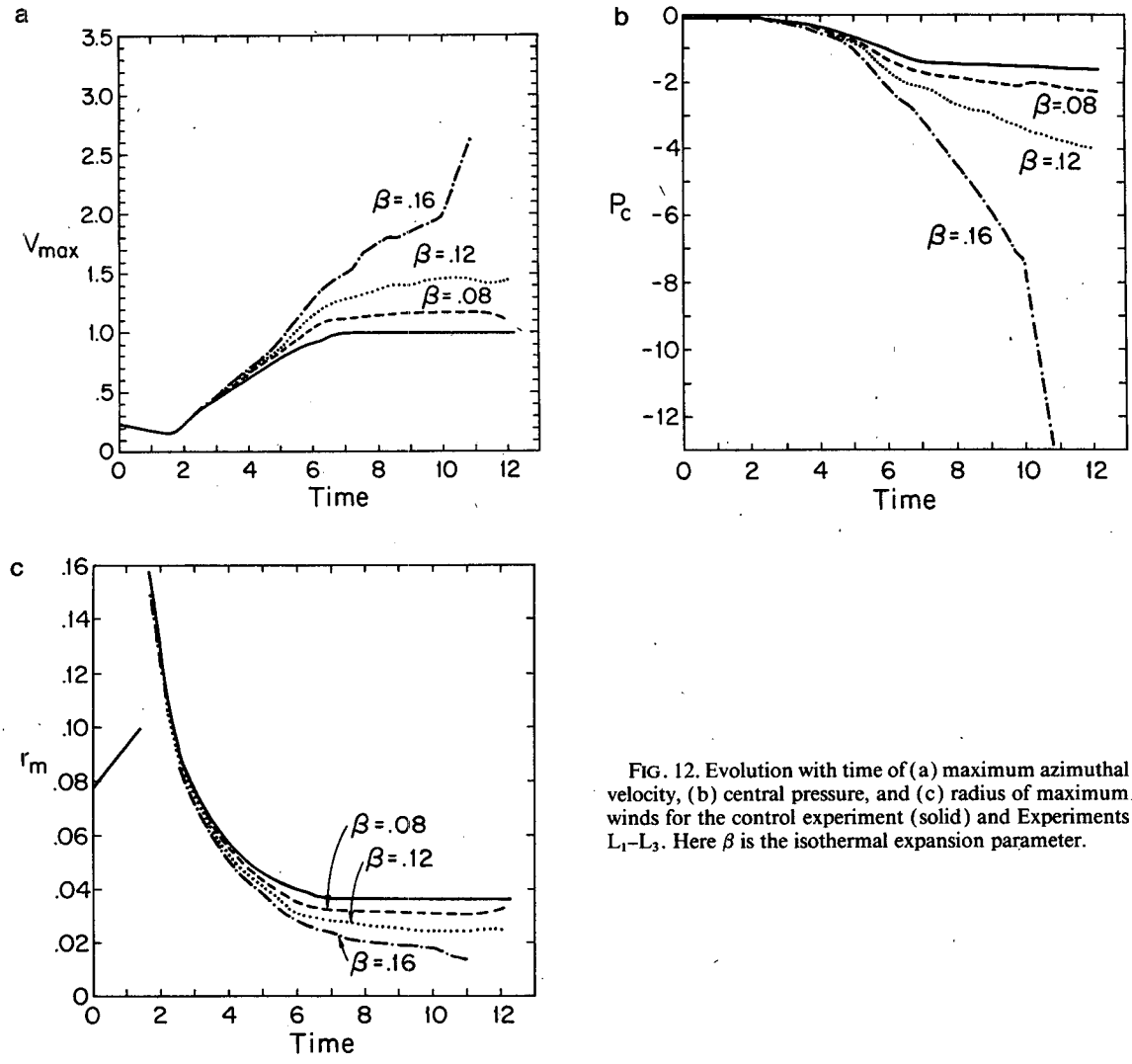

FIG. 12. Evolution with time of (a) maximum azimuthal velocity, (b) central pressure, and (c) radius of maximum winds for the control experiment (solid) and Experiments L_1–L_3. Here β is the isothermal expansion parameter.

(HPE) convection. Other features include the use of Schubert and Hack's potential-radius coordinate, convective adjustment along angular-momentum surfaces, and initialization from a conditionally neutral state.

In the context of this simple model, there is a straightforward explanation for the existence of the threshold amplitude for intensification reported by RE. Ekman pumping first induces upward motion and adiabatic cooling. The initial response of the model to this convective destabilization is to produce LPE clouds. These are ineffective in opposing the adiabatic cooling but maintain convective neutrality by drying out the subcloud layer. The vortex core thus cools and θ_e decreases (by about 2°C in Expt. E) in the subcloud layer. Only when the lower-to-middle troposphere becomes nearly saturated can anomalous surface fluxes counter the drying effect of convective downdrafts to the extent that subcloud-layer θ_e actually increases. This increase is associated with an increase in temperature aloft and thus with an amplification of the cyclone.

An alternative view of this process is illustrated in Fig. 13. The cyclone can only spin up if there is inflow *above* the boundary layer in this model. But the inflowing air is, in the model and in nature, potentially cold (i.e., it has low θ_e). If this air were to simply flow inward and upward, the vortex core would cool. What happens instead is that the lower-tropospheric air follows an indirect route to the tropopause. Before ascending, air above the subcloud layer first descends in convective downdrafts, is moistened by surface evaporation, and finally ascends in deep, HPE convective clouds. Only if fluxes from the ocean succeed in raising the entropy above that of the ambient subcloud layer can the vortex core warm and the cyclone amplify. This view is consistent with the findings of RE. The important limitation on initial growth is the low θ_e of the middle troposphere. Even if the initial ascent is due to processes other than Ekman pumping (e.g., ascent associated with a large-scale wave disturbance) the initial convection will be of low precipitation efficiency

and the argument presented here (see also Fig. 13) pertains.

The LPE clouds are also crucial to the maintenance of an intense vortex. By keeping the subcloud layer relatively dry outside the core, conditional instability to deep convection is reduced and the net upward convective mass flux remains concentrated in the core. In models employing Kuo-type convective representations, deep convection is artificially restrained outside the core by the requirement of moisture convergence; consequently, artificially large conditional instability builds up there.

Other inferences drawn from this work follow:

1) The primary scaling parameter, which controls the amplitude of the azimuthal velocity and pressure, is a measure of the sea–air thermodynamic disequilibrium, χ_s, defined by (38). An upper bound on vortex size is related to the length scale, $\sqrt{\chi_s}/f$. The time scale of evolution and the secondary circulation are controlled by the surface-exchange coefficient as well as by χ_s.

2) The model is not particularly sensitive to the length scale used in the ad hoc eddy viscosity whose thermal component is necessary to prevent frontal collapse in the model. Omitting diffusion of momentum, however, results in only weak development. It appears that momentum diffusion is necessary to spin up the eye, as originally postulated by Malkus (1958) and Kuo (1958).

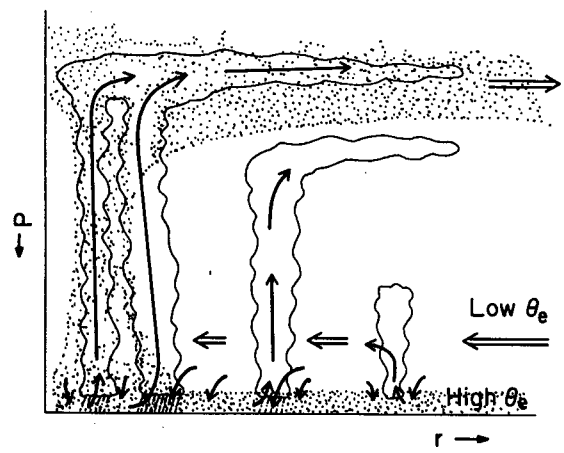

FIG. 13. Air flow in developing tropical cyclone. Dots show high θ_e air. In order for the cyclone to spinup, potentially cold air in the lower troposphere must flow inward. Were it to ascend, the vortex core would rapidly cool and the cyclone would decay. Instead, the potentially cold air descends within shallow clouds, within precipitating downdrafts, and outside of clouds due to Ekman suction. These downdrafts reduce the entropy of the subcloud layer. Only if the surface fluxes are large enough to offset the drying effect of the downdrafts will the subcloud-layer entropy rise above ambient values, enabling the vortex core to become warmer than its environment. In the developing storm, individual air parcels flow inward in the lower troposphere, sink downward in downdrafts, receive entropy from the ocean, and then ascend in deep convective clouds.

3) Consistent with the findings of Emanuel (1986) and RE, the intensity of the mature cyclone is not sensitive to the geometry of the initial vortex, up to an upper limit beyond which amplification is weak. This upper limit is set by the increasing proportion of energy deposited in the upper-level flow as the disturbance size increases. The geometric size of the mature cyclone is strongly related to that of the initiating disturbance.

4) The "incubation period" of the incipient disturbance increases with decreasing relative humidity of the lower troposphere above the subcloud layer. The threshold amplitude for intensification presumably increases as well.

5) Radiative cooling is necessary to maintain a quasi-steady vortex. Its primary function is to permit the subsidence and associated downward advection of dry air necessary to counter the moistening of the outer region by LPE convection. Without radiative cooling, the middle troposphere moistens, deep, HPE convection ultimately develops in the outer region and the vortex expands and weakens.

6) The hurricane subcloud layer is very nearly in equilibrium, even during rapid development.

7) Increasing the isothermal-expansion parameter beyond a critical value appears to lead to runaway intensification, as postulated by Emanuel (1988b).

We note, in closing, that tropical cyclones constitute unique laboratories for probing the nature of cumulus convection. While some of the conclusions presented here are special to tropical cyclones, others may have more general applications. In particular, parcel theory suggests that convection generally exerts a damping influence on temperature perturbations brought about by large-scale processes and causes the subcloud-layer entropy to track free tropospheric temperature changes. Only when convection is coupled with boundary-layer processes such as advection and surface fluxes can it be expected to lead to amplifying large-scale disturbances.

Acknowledgments. The author gratefully acknowledges the support of the National Science Foundation through Grant ATM-8513871. Valuable suggestions were contributed by Richard Anthes, Alan Betts, and Mark Handel. Part of this work was completed while visiting the National Center for Atmospheric Research. The National Center for Atmospheric Research is sponsored by the National Science Foundation.

REFERENCES

Anthes, R. A., 1972a: Non-developing experiments with a three-level axisymmetric hurricane model. NOAA Tech. Memo. ERL NHRL-97, 18 pp.

——, 1972b: The development of asymmetries in a three-dimensional numerical model of a tropical cyclone. *Mon. Wea. Rev.*, **100**, 461–476.

——, 1974: The dynamics and energetics of mature tropical cyclones. *Rev. Geophys. Space Phys.*, **12**, 495–522.

——, 1982: Tropical cyclones: Their evolution, structure and effects. *Meteor. Monogr.*, No. 41, Amer. Meteor. Soc., 298 pp.

Arakawa, A., and W. H. Schubert, 1974: Interaction of a cumulus cloud ensemble with the large-scale environment, Part I. *J. Atmos. Sci.*, **31**, 674–701.

Bergeron, T., 1954: The problem of tropical hurricanes. *Quart. J. Roy. Meteor. Soc.*, **80**, 131–164.

Betts, A. K., 1982: Saturation point analysis of moist convective overturning. *J. Atmos. Sci.*, **39**, 1484–1505.

——, 1983: Thermodynamics of mixed stratocumulus layers; saturation point budgets. *J. Atmos. Sci.*, **42**, 2751–2763.

Byers, H. R., 1944: *General Meteorology.* McGraw-Hill, 645 pp.

Charney, J. G., and A. Eliassen, 1964: On the growth of the hurricane depression. *J. Atmos. Sci.*, **21**, 68–75.

Emanuel, K. A., 1983: The Lagrangian parcel dynamics of moist symmetric instability. *J. Atmos. Sci.*, **40**, 2368–2376.

——, 1986: An air–sea interaction theory for tropical cyclones. Part I. *J. Atmos. Sci.*, **43**, 585–604.

—— 1988a: Observational evidence of slantwise convective adjustment. *Mon. Wea. Rev.*, **116**, 1805–1816.

——, 1988b: The maximum intensity of hurricanes. *J. Atmos. Sci.*, **45**, 1143–1155.

——, and R. Rotunno, 1989: Polar lows as arctic hurricanes. *Tellus*, **41A**, 1–17.

Gray, W. M., 1968: Global view of the origin of tropical disturbances and storms. *Mon. Wea. Rev.*, **96**, 669–700.

Jordan, C. L., 1958: Mean soundings for the West Indies area. *J. Meteor.*, **15**, 91–97.

Kleinschmidt, E., 1951: Grundlagen einer Theorie der tropischen Zyklonen. *Arch. Meteor. Geophys. Bioklim.* **4a**, 53–72. (English translation available from the British Meteorological Office)

Klemp, J., and R. Wilhelmson, 1978: The simulation of three-dimensional convective storm dynamics. *J. Atmos. Sci.*, **35**, 1070–1096.

Kuo, H. L., 1958: Dynamics of convective vortices and eye formation. *The Atmosphere and the Sea in Motion*, B. Bolin, Ed., Rockefeller Institute Press, pp. 413–424.

——, 1965: On formation and intensification of tropical cyclones through latent heat release by cumulus convection. *J. Atmos. Sci.*, **22**, 40–63.

Malkus, J. S., 1958: On the structure of the mature hurricane eye. *J. Meteor.*, **15**, 337–349.

Merrill, R. T., 1984: A comparison of large and small tropical cyclones. *Mon. Wea. Rev.*, **112**, 1408–1418.

Ooyama, K., 1964: A dynamical model for the study of tropical cyclone development. *Geofis. Int.*, **4**, 187–198.

——, 1969: Numerical simulation of the life cycle of tropical cyclones. *J. Atmos. Sci.*, **26**, 3–40.

Raymond, D. J., 1983: Wave-CISK in mass flux form. *J. Atmos. Sci.*, **40**, 2561–2572.

Riehl, H., 1954: *Tropical Meteorology.* McGraw-Hill, 392 pp.

Rotunno, R., and K. A. Emanuel, 1987: An air-sea interaction theory for tropical cyclones. Part II. *J. Atmos. Sci.*, **44**, 542–561.

Schubert, W. H., and J. J. Hack, 1983: Transformed Eliassen-balanced vortex model. *J. Atmos. Sci.*, **40**, 1571–1583.

Xu, K., and K. A. Emanuel, 1989: Is the tropical atmosphere conditionally unstable? *Mon. Wea. Rev.*, **117**, 1471–1479.

Yanai, M., 1964: Formation of tropical cyclones. *Rev. Geophys.*, **2**, 367–414.